Copy
RM E54A07

NACA RM E54A07

NACA

RESEARCH MEMORANDUM

PRESSURE RECOVERY AND MASS-FLOW PERFORMANCE OF FOUR ANNULAR NOSE INLETS OPERATING IN MACH NUMBER REGION OF 3.1 AND REYNOLDS NUMBER RANGE OF APPROXIMATELY 0.45×10^6 TO 2.20×10^6

By Henry R. Hunczak

Lewis Flight Propulsion Laboratory
Cleveland, Ohio

NATIONAL ADVISORY COMMITTEE
FOR AERONAUTICS

WASHINGTON
March 26, 1954

NATIONAL ADVISORY COMMITTEE FOR AERONAUTICS

RESEARCH MEMORANDUM

PRESSURE RECOVERY AND MASS-FLOW PERFORMANCE OF FOUR ANNULAR NOSE INLETS OPERATING IN MACH NUMBER REGION OF 3.1 AND REYNOLDS NUMBER RANGE OF APPROXIMATELY 0.45×10^6 TO 2.20×10^6

By Henry R. Hunczak

SUMMARY

Four annular nose inlets that covered a wide range of supersonic compression were investigated to determine the effect of Reynolds number on their pressure recovery and mass-flow performance. The studies were conducted over a range of angles of attack with various geometric modifications to the basic inlets.

The effect of increasing the Reynolds number was to improve the performance of the configurations with internal contraction and to reduce the performance of the isentropic inlet with no internal contraction; the major change in performance occurred in the Reynolds number range below 1.20×10^6.

Two inlets, both of the isentropic type, attained pressure recoveries of 0.77, which is representative of the upper limit attainable with current inlet designs in this Mach number region.

INTRODUCTION

Supersonic nose inlets with multiple oblique shocks generated by a properly contoured central body were investigated in the Mach number region of 3.0 as early as 1944 (ref. 1). Since that time, numerous analytical and experimental studies on the problem of attaining efficient supersonic compression have been conducted and a considerable amount of data accumulated. Some of the more recent investigations are listed in references 2 to 6.

Experience since the earliest investigations indicates that as the Mach number increases the pressure recovery, mass flow, and stable subcritical flow regulation become increasingly sensitive to

slight inlet geometry changes in that they tend to diverge further below the theoretical expectations based on the assumption of non-viscous flow. The majority of this discrepancy is currently attributed to the higher adverse pressure gradients encountered with the increase in compression which promotes boundary-layer growth and separation, especially the separation encountered in shock boundary-layer interaction. It may therefore be expected that the Reynolds number may have a pronounced effect on the over-all inlet operation if the state of the boundary layer were appreciably altered.

Accordingly, in the present study made in the Mach number region of 3.1, four annular nose inlets covering a wide variation in the degree of supersonic compression were investigated first at an inlet Reynolds number of approximately 0.45×10^6 over a range of spike tip positions and angles of attack from zero to 10°. This phase of the investigation was made to determine the effect of inlet geometry changes on the performance. The performance of the inlets was then determined over a range of Reynolds numbers from 0.45×10^6 to 2.20×10^6 at both zero and 4.9° angles of attack for selected values of spike-tip positions.

SYMBOLS

The following symbols are used in this report:

H	stagnation pressure, lb/sq in.
m	mass flow, slugs/sec
Re	Reynolds number based on inlet diameter of cowl
x	axial distance from spike tip, in.
α	angle of attack, deg
θ_l	spike-tip position, angle between axis of symmetry and line from spike apex to cowl lip, deg

Subscripts:

i	projected area of cowl inlet without centerbody
s	cone surface

0 free stream (fig. 1)

3 diffuser exit (fig. 1)

4 exit of movable plug (fig. 1)

APPARATUS AND TEST PROCEDURE

The four annular nose inlets investigated, listed in order of increasing supersonic compression, were (1) a 1-cone 44° spike with internal contraction, (2) a 2-cone 40° to 70° spike with internal contraction, (3) an isentropic spike with internal contraction, and (4) an isentropic spike with no internal contraction.

For each inlet, at least one modification of the spike or cowling was tested. For convenience, the inlets will be referred to as I, II, III, and IV, respectively, along with the subscripts a, b, and c to designate the various spikes and/or cowlings within each type. The coordinates of these cowlings and spikes (centerbodies) are presented in tables I to IV. The external cowl-lip angles were held to a value not more than 4° or 5° greater than the internal-lip angle. Inasmuch as all inlets were required to discharge to a common diameter, the cowl diameters at the lip ranged from 3.00 to 3.38 inches to satisfy desired rates of internal cowl curvature. Unless otherwise specified, the external contours were faired arbitrarily to a diameter of $4\frac{1}{2}$ inches. No attempt was made to maintain a minimum wall thickness since external drag was not a part of the investigation.

The design of the 1-cone inlet (inlet I) was based on the information contained in reference 2 for the 4°,7° cowling (4° internal, 7° external cowl-lip angle) in combination with a 22° cone half-angle spike having a ratio of maximum spike-to-cowl-lip diameter of 0.834. In reference 2 this configuration gave close to the maximum pressure recovery of all configurations investigated at a Mach number of 3.30, and the data indicated that good performance was also attainable at a Mach number of 3.05. The internal contraction was such that only a small reduction in centerbody diameter would be required to permit starting at a Mach number of 3.05. Accordingly, the cowling of inlet I had an internal contour geometrically similar to the 4°,7° cowling of reference 2, and the three centerbodies had initially 22° half-angle cones.

The geometry of spike I_a between the tip and the maximum diameter was similar to that in reference 2. Downstream of the maximum diameter

the contour was modified from that in reference 2 to provide a matching-area variation with the afterbody, which had an initial half-angle taper of 2.84°. This taper gives a diffusion rate approximately that of a 5° conical divergence. Spike I_b was obtained by decreasing the diameter of spike I_a by 0.068 inch to relieve the internal contraction and to permit starting at a Mach number of 3.05. Spike I_c was designed with a more gradual rate of internal compression from that in reference 2 to reduce pressure gradients in the boundary layer.

Inlet II had spikes with 20° to 35° half-angle cones. Spike II_a was designed so that the internal contraction was close to the maximum permissible for supersonic flow into the inlet when the oblique shock was slightly ahead of the cowl. Spike II_b was obtained by reducing the maximum diameter by 0.60 inch to relieve the internal compression.

Inlet III had an initial half-angle cone of 15° followed by an isentropic compression surface which was designed to focus all compression waves at the cowl lip. The Mach number at the surface was reduced theoretically to 1.76 prior to internal compression. With this spike surface Mach number, it was possible to attain supersonic flow into the inlet with an attached shock at the cowl lip. For spike III_a the maximum amount of internal compression was used. For spike III_b the internal contraction was reduced by decreasing the diameter of the centerbody 0.082 inch.

Inlet IV also had an initial half-angle cone of 15° followed by an isentropic compression surface which focused all compression waves at the cowl lip. The spike surface Mach number was reduced to 1.50. The internal contour of cowl IV_a was designed to collect the flow smoothly at the lip and to diffuse it gradually with no supersonic internal compression. The external contour, as previously mentioned in this section, was arbitrary, except that the external lip angle was 4° greater than the internal lip angle and exceeded the detachment angle of the free-stream Mach number. For cowl IV_b, the external contour of cowl IV_a was remachined to a thinner and more realistic thickness to reduce the cowl projected area in the subsonic flow field behind the detached shock and thus minimize the interference between the external and internal flow. However, for both cowls IV_a and IV_b the initial lip angle was the same.

Two spikes were investigated with cowling IV_a. The first, spike IV_a, had a solid surface, while the second, spike IV_b, had a porous surface which was fabricated from sintered bronze. The porosity

extended from the tip to the maximum diameter and permitted a continuous boundary-layer suction along the spike surface. Because the technique of fabricating sintered bronze is in the experimental stage, the contours varied a maximum of ±0.015 inch from the theoretical along the isentropic compression surface. In addition, the tip section was elongated approximately 0.1 inch.

A method of influencing the compression-surface boundary layer was the use of roughness in the form of number 60 or 80 carborundum grit on several of the spike tips or surfaces to induce in the boundary layer a transition from laminar to turbulent flow.

All inlets were investigated with the same test support body and diffuser. In figure 1 a scale drawing of the test apparatus is shown with a 1-cone inlet installed. Figure 2 is a photograph of the model suspended in the tunnel. The tubes mounted alongside the diffuser support body are collectors for the boundary-layer bleedoff air which passes through the hollow centerbody and support struts. In the present investigation, these collector tubes were vented to the free stream as shown. The spacers behind the cowling permitted variation of the spike-tip projection in increments of 0.025 inch. The spike-tip projection is presented in terms of the tip position θ_l. The value of this parameter increases as the spike tip is retracted toward the cowl lip.

The pressure at the diffuser exit was measured with a 40-tube pilot rake. The pressure recoveries as presented are averages based on an area weighting. The mass flow passing through the model was calculated by using the total-pressure recovery at station 3 and the sonic exit area at the movable plug at station 4 (see fig. 1). This mass-flow measuring technique was calibrated with inlets capturing a full-stream tube of air. The calibration factor thus obtained was incorporated in the calculations.

The investigation was conducted in two tunnels. The 18- by 18-inch supersonic wind tunnel operated at a Mach number of 3.05 at the diffuser inlet as determined by a wedge calibration and at a Reynolds number of 1.70×10^6 per foot. The stagnation temperature of the air was held at 150° F and the dew-point temperature was maintained at -10° to -30° F. The inlets were investigated over a range of spike-tip positions by varying the cowl spacers.

The 1- by 1-foot supersonic wind tunnel was operated at a Mach number of 3.13 over a range of stream Reynolds numbers from 1.70×10^6 to 8.0×10^6 per foot. The stagnation temperature varied between 50° and 65° F and the dew-point temperature was maintained at less than -40° F. Inlet designs were investigated at one or two values of the spike-tip position and at zero and 4.9° angles of attack.

RESULTS AND DISCUSSION

Inlet performance is presented in terms of the pressure recovery and captured-mass-flow ratio at flow conditions corresponding to critical flow, peak pressure recovery, and minimum stable flow. Peak pressure recovery is defined as the ratio of the maximum stagnation pressure attained at the diffuser exit divided by the free-stream stagnation pressure. The captured-mass-flow ratio m_3/m_1 is the ratio of the mass flow passing through the model divided by the mass flow passing through a free-stream tube equal in area to that of the cowl inlet without a centerbody. The Reynolds number is based on the diameter of the cowl lip. Although at a stream Reynolds number of 1.70×10^6 the inlet Reynolds number ranged from 0.42×10^6 to 0.48×10^6, this slight variation is neglected and an average value of 0.45×10^6 is used throughout.

Inlet Performance Over Range of Spike-Tip Positions

The effect on the inlet performance characteristics of variations in spike-tip position is shown in figures 3 to 6 for a free-stream Mach number of 3.05, zero angle of attack, and a Reynolds number of approximately 0.45×10^6.

Attached shocks at the cowl lips were obtained for inlets I, II, and III unless the flow was overcontracted or the boundary layer separated. Shock detachment is noted by the sudden break in the curves of the captured-mass-flow ratios at high values of spike-tip position. Stable subcritical operation was obtained only when the inlets were overcontracted or the internal contraction was nominal, in which case subcritical operation could be entered into without too severe an expulsion of the terminal shock wave.

The performance of spike I_a (rapid internal contraction and smooth) was reduced below that of spike I_c (fig. 3(a)) by an oscillating separation of the boundary layer that persisted for all supercritical values of pressure recovery and captured-mass-flow ratio attainable. This type of instability was not the usual buzz phenomenon encountered in subcritical operation in that the separation did not travel to the spike tip and severe pulsations with flow reversal through the diffuser were not evident. It was also obtained with spike I_b smooth (data not shown) and is believed to be caused by the high-pressure gradient of the rapid internal contraction. Tip roughness stabilized the boundary layer for both spikes with a resultant improvement in performance (fig. 3(b)), although the flow for spike I_a was detached. The

maximum pressure recovery of 0.55 obtained with spike I_a was approximately 10 percent below that predicted for a Mach number of 3.05 from the experimental data of reference 2.

For inlets II and III (with internal contraction) the peak pressure recovery did not improve substantially with increasing spike-tip position in the region where the cowl lip approaches the oblique shock from the spike tip, although such an improvement would be expected from theoretical considerations based on nonviscous flow because of the increases in internal contraction. This lack of improvement was most evident for spikes II_b and III_b (figs. 4 and 5) where the pressure recovery remained constant or decreased, although the gains in captured-mass-flow ratio indicated that the cowl lip had not moved upstream of the spike-tip shock. However, the effectiveness of internal contraction by changing the centerbody diameter is indicated by the loss in pressure recovery when the diameters of spikes II_a and III_a were reduced to II_b and III_b, respectively.

The critical captured-mass-flow ratio of cowl IV_a was comparable with that of cowl IV_b for spike-tip positions less than θ_l of 25.07°. The thinner lip of cowl IV_b, however, permitted a greater mass-flow ratio to be obtained by increasing the spike-tip position to 25.22°. Also, the peak pressure recovery of approximately 0.77 occurred at a higher captured-mass-flow ratio, which conformed more closely with the theoretical expectations. Subcritical stability was obtained over the entire range of cowl spacers but was appreciable only after a sharp break in the mass-flow-ratio curve.

Both inlets III and IV attained maximum pressure recoveries of approximately 0.77. This recovery is representative of the upper limit attained with current inlet designs at a Mach number of 3.10.

Inlet Performance at Angle of Attack with and without Spike-Tip Roughness

At a Mach number of 3.05 and a Reynolds number of approximately 0.45×10^6, the performance at angle of attack is shown in figures 7 to 10 for selected values of spike-tip position which gave close to the best performance at zero angle of attack. As the angle of attack was increased from zero to approximately 10°, all configurations eventually suffered losses in performance. These losses are believed to arise from (1) a reduction in supersonic compression on the lee side of the inlet as a result of the asymmetrical alinement of the spike to the free-stream flow, (2) boundary-layer cross flow and accumulation in the lee side of the spike which may modify the shock

pattern adversely and aggravate separation, and (3) flow angularities at the inlet throat.

For inlets I and II the marked changes in performance (figs. 7 and 8) which were obtained with the addition of tip roughness could be associated with the observed alterations of the boundary-layer flows and shock patterns. For inlets III (fig. 9) and IV (data not shown) tip roughness altered the observed boundary-layer flow only slightly, and the performance was relatively unaffected.

Specifically, the rapid deterioration of performance for inlet I with a smooth tip (fig. 7) at angles of attack above 6° was associated with what appeared to be a rapid accumulation of boundary layer on the lee surface of the spike which eventually covered one entire side of the inlet. Below a 6° angle of attack this boundary-layer accumulation was gradual, and relatively constant inlet performance was attained. Tip or cone-surface roughness generated a boundary layer that was presumably turbulent since it resisted crossflow, as evidenced by an apparent uniformity in thickness about the spike surface at angle of attack, and also did not exhibit the extensive thickening ahead of the cowl at zero angle of attack. Although a reduction in internal contraction by reducing the spike-tip position was required to maintain attached shocks at the cowl lip, a maximum pressure recovery of 0.58 was obtained at zero angle of attack, and both peak pressure recovery and captured mass-flow ratio were appreciably improved above a 7.5° angle of attack. Below a 7.5° angle of attack the pressure recovery was increased at the expense of a reduction in mass flow.

Inlets with internal contraction experienced a large reduction in performance caused by an abrupt separation of the flow from the entire lee surface of the spikes at the higher angles of attack. (This type was also encountered in ref. 7.) The tendency of the boundary layer to separate was alleviated by adding roughness to the tip for spike I_a and by a reduction in spike-tip position θ_l for spikes II and III.

The effect of spike-tip roughness on the peak pressure recovery of spikes II_a and II_b was unpredictable. However, its effect on the captured-mass-flow ratio in the vicinity of zero angle of attack could be correlated qualitatively with its influence on the shock pattern for various spike-tip positions through the following considerations. Spikes II_a and II_b with a smooth tip had boundary layers which separated and reattached (bridged) across the 15° discontinuity (20° to 35°) in the spike surface. This type of bridging, which has been experienced in many previous investigations, is generally associated with a laminar boundary layer. It generates a weak oblique shock eminating from the separation point and transposes

the stronger shock eminating from the spike discontinuity rearward to the reattachment point. Tip roughness eliminated the boundary-layer bridging so that only a single strong oblique shock, that from spike discontinuity, accomplishes the required 15° flow turning where formerly two shocks existed. Because the oblique shocks deflect the flow outward from the spike axis and the amount of flow deflection is a function of shock strength, both the shock intensity and the number and position of the shocks ahead of the cowl lip determine the flow spillage. At θ_l of 28.61° (spike II_a, smooth (fig. 8(a)), the spike-tip shock and the weak boundary-layer-separation shock were ahead of the cowl lip and the reattachment shock fell inside. With tip roughness both the tip shock and the stronger discontinuity shock fell ahead of the cowl lip and the flow spillage was increased. With a retraction of the spike to θ_l of 29.23° (spike II_b, smooth (fig. 8(b)), the tip and separation shocks were still ahead of the inlet with no tip roughness. The discontinuity shock obtained with tip roughness fell at the cowl lip, however, resulting in a net gain in the captured-mass-flow ratio. At θ_l of 29.65, all shocks fell at or inside the cowl lip for both the smooth and rough tip so that the captured mass flow remained unchanged (within the precision of measurement) for at least a zero angle of attack.

As previously indicated in this section, the performance of inlets III and IV was relatively unaffected by tip roughness (fig. 9, spike III_b) with the exception that the peak pressure recovery was reduced slightly for spikes III_a and IV_a (data not shown) at zero angle of attack. For inlet IV (fig. 10) the performance was affected primarily by the change in the wall thickness of the cowl. Although the pressure recovery remained essentially the same, the critical captured-mass-flow ratio for cowl IV_b was substantially greater that that of cowl IV_a over the range of angles of attack.

Effect of Stream Reynolds Numbers on Inlet Performance

In order to determine the effect of stream Reynolds number on inlet performance, selected inlets were investigated over a Reynolds number range from approximately 0.45×10^6 to 2.20×10^6 at a Mach number of 3.13 for zero angle of attack. The data at a 4.9° angle of attack are also presented as a matter of interest. For some configurations, spike-tip roughness was also used.

At zero angle of attack the general effect of increasing the Reynolds number was to improve the performance of inlets I, II, and III and to reduce the performance of inlet IV, with the major changes occurring in the Reynolds number range below approximately 1.20×10^6

(figs. 11 to 15). In this range, increasing the Reynolds number altered the apparent boundary-layer thickness, the tendency to bridge, and the resulting shock pattern.

For the 1-cone inlet (fig. 11(a)) the performance was independent of Reynolds number effects as long as the boundary layer along the spike surface appeared turbulent. This turbulence was attained either by increasing the Reynolds number or by the addition of tip roughness. For spike I_a with tip roughness, the performance remained constant over the entire range of Reynolds numbers investigated. For spike I_c smooth, peak recovery increased progressively in the Reynolds number range of 0.45×10^6 to 1.20×10^6. For spike I_a smooth, an abrupt transition from a separated oscillating boundary layer to a steady turbulent boundary layer occurred at a Reynolds number of 1.20×10^6. This stabilizing influence of turbulence on the boundary layer was the same phenomenon as that which occurred at a Mach number of 3.05. However, at the higher Mach number of 3.13 the shocks at the cowl lip were attached for spike I_a, and a captured-mass-flow ratio of approximately 1.0 was attained.

For the 2-cone inlet, the performance improved with increasing Reynolds number, but the peak pressure recovery was reduced by tip roughness over the entire range of Reynolds numbers investigated (fig. 12). This adverse effect of tip roughness is in contrast with that obtained with the 1-cone inlet and cannot be explained on the basis of observed boundary-layer turbulence and oblique-shock pattern alone. In the case of spike II_a smooth, the three-oblique-shock pattern formed by a laminar boundary-layer bridge which occurs at the Reynolds number of 0.45×10^6 should be more isentropic than the two-oblique-shock pattern formed when the boundary-layer turbulence was increased by raising the Reynolds number to 2.14×10^6. In addition, the reduction in pressure recovery which occurred when turbulence was obtained by tip roughness is inconsistent with the Reynolds number effect if only changes in shock pattern are considered. These results indicate that a more comprehensive knowledge of the boundary-layer flow is required to explain the effect of turbulence on the pressure recovery and that the slight changes in oblique-shock structure are of secondary importance. This contention is further substantiated by the data for inlets III (fig. 13) and IV (fig. 14). For inlet III a reduction in pressure recovery with the addition of tip roughness was obtained, and for inlet IV a reduction in pressure recovery with increasing Reynolds number was obtained, although in both cases the corresponding supersonic-flow fields appeared to be more isentropic.

The variation in critical captured-mass-flow ratio for inlet IV with spike-tip positions of 24.76° and 24.91° and the improvement in subcritical stability as the Reynolds number was raised are presented in figure 14. At the Reynolds number of 0.45×10^6, the change in inlet performance as the spike-tip position was increased from 24.76° to 24.91° was similar to that occurring at a Mach number of 3.05. For both tip positions and Mach numbers, the subcritical stability of approximately 1 percent of the critical flow was nominal. At a Reynolds number of approximately 1.1×10^6 or above, the critical captured-mass-flow ratio for θ_l of 24.76° equaled that obtained with θ_l of 24.91°. In addition, the subcritical stability for θ_l of 24.91° was substantially improved to approximately 8 percent of the flow by increasing the Reynolds number; the stability for θ_l of 24.76° also showed improvement. These results indicate that the selection of the optimum tip position from data at a low Reynolds number may be erroneous for a similar configuration to be operated at a higher Reynolds number. To determine the reasons for a reduction in supercritical captured-mass-flow ratio with increasing Reynolds number would require a more comprehensive investigation of the boundary layer and flow field; however, this trend does imply an increasing upstream displacement of the external detached cowl-lip shock with increasing Reynolds number.

The effect of spike-tip roughness (fig. 15(a)) and continuous boundary-layer suction (fig. 15(b)) on the inlet performance was to suppress the reduction in performance with increasing Reynolds number experienced with spike IV_a smooth. Although both methods of altering the boundary-layer flow were detrimental to the inlet performance at a Reynolds number of 0.45×10^6, they became increasingly beneficial at Reynolds numbers above 0.80×10^6. In either case, the trends are such that at the Reynolds number of 0.45×10^6 neither method approximated the effect of high Reynolds number on the performance of spike IV_a smooth.

The subcritical stability of spike IV_a with tip roughness and IV_b also improved with increasing Reynolds number. However, the stability obtained with either configuration was less than that obtained for spike IV_a smooth in the Reynolds number range above approximately 0.80×10^6. The better stability of spike IV_a smooth is opposed by the better pressure recovery of spike IV_b and spike IV_a with tip roughness, which indicates that in this instance the desirable boundary-layer flow conditions for the two were not related.

The relative amount of boundary-layer removal should not be determined from a comparison of the critical mass flows of spike IV_b with that of spike IV_a smooth. The porous surface of spike IV_b was rough and generated disturbances similar to those of spike IV_a with tip roughness. Therefore, a more reasonable estimate of the boundary-layer removal would be a comparison of the curve of critical captured-mass-flow ratio for spike IV_b with that of IV_a with tip roughness. If this is done, the amount of boundary-layer removal at a Reynolds number of 0.45×10^6 is approximately 0.5 percent of the flow entering the inlet and increases to approximately 2.5 percent at a Reynolds number of 1.10×10^6.

At a Reynolds number of 0.45×10^6, a comparison of the peak pressure recoveries obtained at a Mach number of 3.05 with those at a Mach number of 3.13 disclosed a reduction in performance, only a part of which can be attributed to the increase in Mach number. The magnitude of the reduction ranged from approximately 8 percent for the 1-cone inlet to 11 percent for the isentropic inlet with no internal contraction. In this connection, recent unpublished data indicate that the turbulence level of the stream flow may be a factor producing this result. At the time of the investigation, preliminary surveys indicated that the turbulence level of the Mach 3.13 tunnel was considerably higher than that of the Mach 3.05 tunnel and it varied with stream Reynolds number per foot. The effect of the turbulence level on the results of the present study is unknown.

Spike Surface Static-Pressure Distributions

The static-pressure distributions taken axially along the isentropic spike surfaces gave an indication that the variation in diffuser peak pressure recovery with spike-tip position and Reynolds number was a result of internal boundary-layer separation or shock boundary-layer interaction and not a result involving a change in the oblique-shock pattern upstream of the inlet lip or of terminal shock stability.

In figures 16 to 19 the data show that the static-pressure distributions upstream of the cowl lip for both inlets III and IV were not influenced to a large extent by either a change of internal compression or a variation of inlet geometry, and only to a small extent by a change in Reynolds number except at a station located in the vicinity of the detached wave from the cowl lip for inlet IV. At the end of the isentropic curvatures, the measured static-pressure ratios of 6.8 at $x = 3.0$ inches for inlet III (fig. 16) and 10.4 at

x = 3.45 for inlet IV (fig. 18) are in good agreement with the theoretical values of 6.9 and 10.6, respectively, for a Mach number of 3.05. These data indicate that the variations in peak diffuser pressure recovery originated from causes that occur downstream of these points on the spike.

For inlet III (figs. 16(b) and 17) the large rise in static pressure that originated at or downstream of the cowl lip is of the same order of magnitude as would be expected downstream of the terminal shocks (measured; $p_s/p_0 \approx 23$; theoretical; $p_s/p_0 \approx 26.0$) The majority of this static-pressure rise was accomplished forward of the geometric throat and indicates not only that the boundary layer has modified the flow area of the inlet geometry but that the requirement of shock stability at the minimum area for optimum pressure recovery was satisfied and therefore was not a factor causing the variation in pressure recovery with cowl spacers or Reynolds number. Shock stability may also be ruled out as a factor influencing pressure recovery in the case of inlet IV, in which the diffuser pressure recovery decreased with Reynolds number although the subcritical shock stability was improved (see fig. 14(a)). Instead of depending on shock stability, for both inlets III (fig. 17) and IV (fig. 19) the variation of pressure recovery with Reynolds number seemed to be associated with a break in that portion of the static-pressure-distribution curve attributed to the terminal shocks. This loss is located in the vicinity of the spike shoulder and implies a boundary-layer separation. In this connection, the curvature of the spike shoulder and/or the location of the terminal shocks relative to the spike shoulder may be of importance, as indicated in reference 8.

Inlet Schlieren Photographs

Schlieren photographs showing the various spike boundary layers and shock patterns for inlets I, II, III, and IV are presented in figures 20 to 24. At a Reynolds number of 0.45×10^6, a Mach number of 3.05, zero angle of attack, and with no cowl, the boundary layer along the surface of spike I_c appeared to be thin (fig. 20(a)). Installation of the cowling produced what appeared to be a noticeable thickening of a laminar boundary layer ahead of the cowl lip (fig. 20(b)). This thickening of the boundary layer persisted at all values of the pressure recovery and was therefore believed to be a result of the adverse pressure gradient caused by the internal contraction.

The separated oscillating boundary layer of spike I_a smooth is shown in figure 20(c). The photograph taken at 1/100 second is blurred because of the rapid movements of the flow structure. The

nature of the boundary-layer instability may be seen in figure 20(d), a schlieren photgraph taken at a 2-microsecond exposure. The instability appears to be an asymmetrical separation of the boundary layer which at the instant of exposure occurred at the top surface of the spike. With tip roughness, the boundary layer for spike I_c appeared turbulent (fig. 20(e)) and that of spike I_a was stabilized. An increase in Reynolds number to or above 1.20×10^6 produced similar results for spike I_a smooth (see fig. 20(f) at a Reynolds number of 1.26×10^6).

The marked difference in spike boundary layer at angles of attack between spike I_c smooth and spike I_c with tip roughness may be seen in the schlieren photographs of figure 21. For spike I_c smooth the boundary layer gradually shifted to the lee side at small angles of attack (fig. 21(a)). As the angle of attack was increased, the boundary layer on the lee side of the spike increased in thickness (fig. 21(b)) and separated (fig. 21(c)) until at an angle of attack of 10° it filled one side of the inlet (fig. 21(d)).

With tip roughness, spike I_c maintained what appeared to be a relatively uniform boundary-layer distribution up to an angle of attack of 8.3° (fig. 21(e)). However, at an angle of attack of 10.3° (fig. 21(f)), an abrupt separation from the spike surface occurred on the lee side of the spike.

Schlieren photographs of the 2-cone inlet are presented in figure 22. At a Reynolds number of 0.45×10^6 the additional oblique shock generated by the boundary-layer bridge can be seen upstream of the spike break (fig. 22(a)). The amount of bridging decreased with Reynolds number until at a value of 2.13×10^6 it became negligible (fig. 22(b)). The effect of angle of attack and tip roughness on the boundary layer may be seen in figures 22(c) and (d). As the angle of attack was increased, the boundary-layer bridge across the spike break was reduced on the windward side and increased on the lee side (fig. 22(c)). The addition of tip roughness effectively prevented boundary-layer separation as seen in figure 22(d). These results are similar to those obtained in reference 7 at a Mach number of 3.85.

At zero angle of attack, a Mach number of 3.05, and a Reynolds number of 0.45×10^6, inlet III had an oblique shock generated by what appeared to be a laminar boundary-layer separation in figure 23(a). Another shock then occurred at the point of reattachment. For the same configuration with tip roughness, the boundary layer appeared attached along the complete external length of the spike and the flow pattern appeared more isentropic (fig. 23(b)).

Schlieren photographs of cowls IV_a and IV_b at a Mach number of 3.05 are presented in figures 24(a) and (b) for supercritical diffuser operation. Besides the boundary-layer bridging which occurred on the spike surface with both cowls, it will be noticed that the detached wave ahead of cowl IV_a is stronger and displaced further upstream of the cowl lip than that ahead of cowl IV_b.

SUMMARY OF RESULTS

Four annular nose inlets were investigated at a Mach number of 3.05, a Reynolds number of approximately 0.45×10^6, and a range of angle of attack from zero to 10°, and at a Mach number of 3.13, a range of Reynolds numbers from approximately 0.45×10^6 to 2.20×10^6, and at angles of attack of zero and 4.9°. In order of increasing supersonic compression, a 1-cone 44° spike, a 2-cone 40° to 70° spike, and an isentropic spike inlet (all having internal contraction) were designed and operated with attached shocks at the cowl lips. An isentropic inlet with no internal contraction and operating with detached shocks at the cowl lips had the highest supersonic compression.

In addition to contributing to the general knowledge of the performance attainable for a succession of inlets that cover a wide range of compression, the following results were obtained:

1. The peak pressure recovery and relative mass flow were most affected by changes in Reynolds number in the range below 1.20×10^6. The inlets with internal contraction exhibited an improvement in performance with Reynolds number, and the isentropic inlet with no internal contraction exhibited a reduction in performance.

2. As deduced from flow observations, the visible effect of an increase in Reynolds number and/or roughness on the tip of the centerbody was to induce an early transition from laminar to turbulent flow in the boundary layer. For the 1-cone inlet with a gradual internal contraction, this early transition eliminated what appeared to be a rapid thickening in the vicinity of the cowl lip of a presumably laminar boundary layer. For the 1-cone inlet with rapid internal contraction, the early transition attached and stabilized an otherwise separated oscillating boundary layer. In both cases the performance was markedly improved. For the 2-cone and isentropic inlets the early transition reduced or eliminated boundary-layer bridging, but the change in external shock structure was found to be of secondary importance in influencing the peak diffuser pressure recovery. Except for the 1-cone inlet, tip roughness could not be used at a low Reynolds number to simulate inlet operation at a higher Reynolds number.

3. The subcritical stability of inlets with internal contraction was negligible unless the cowl was positioned so that the internal contraction either generated detached shocks at the cowl lip for supercritical values of mass flow or unless the internal contraction was nominal. For the inlet with no internal contraction, a change in Reynolds number from 0.45×10^6 to 1.11×10^6 increased the mass-flow subcritical stability range from 1 to 8 percent. For the same inlet, either tip roughness or continuous boundary-layer suction along the centerbody surface forward of the maximum diameter improved the subcritical stability at Reynolds numbers below 0.80×10^6 but reduced it at the higher Reynolds numbers.

4. Two inlets, both of the isentropic type, attained peak pressure recoveries of 0.77. This peak pressure recovery is representative of the upper limit attainable with current inlet designs in the Mach number region of 3.10.

Lewis Flight Propulsion Laboratory
National Advisory Committee for Aeronautics
Cleveland, Ohio, January 14, 1954

REFERENCES

1. Oswatitsch, Kl.: Pressure Recovery for Missiles with Reaction Propulsion at High Supersonic Speeds (The Efficiency of Shock Diffusers). NACA TM 1140, 1947.

2. Ferri, Antonio, and Nucci, Louis M.: Theoretical and Experimental Analysis of Low-Drag Supersonic Inlets Having a Circular Cross Section and a Central Body at Mach Numbers of 3.30, 2.75, and 2.45. NACA RM L8H13, 1948.

3. Dailey, C. L.: Development of Supersonic Ramjet Diffusers. Summary Rep. under Item 1, USCAL Rep. 8-1, Aero. Lab., Univ. Southern Calif., Jan. 10, 1951. (U.S. Navy Bur. Aero. Contract NOa(s) 9961, Item 1.)

4. Pearce, R. B.: Tests of Multishock Diffusers. Rep. No. AL1117, Proj. MX-770, North American Aviation, Inc., Sept. 21, 1950.

5. Clark, Donald B., and Lewis, Robert B.: Development of Wide Range Supersonic Inlets. Wright Aeronautical Corp.

6. Stoolman, Leo, and Francis, Donald L.: Supersonic Diffuser Performance With and Without Combustion. JPL Preprint, Jet Prop. Lab., C.I.T., Sept. 18, 1950.

[redacted]

7. Connors, James F., and Woollett, Richard R.: Performance Characteristics of Several Types of Axially Symmetric Nose Inlets at Mach Number 3.85. NACA RM E52I15, 1952.

8. Connors, James F., and Woollett, Richard R.: Some Observations of Flow at the Throat of a Two-Dimensional Diffuser at a Mach Number of 3.85. NACA RM E52I04, 1952.

TABLE I. - 44° SPIKE INLET, I

	Spike I_a	Spike I_b	Spike I_c	Cowl	
Coordinates, in.					
x	y	y	y	x (internal)	y (internal)
0	0	0	0	0	1.690
.50	.200	.200	.201	.25	1.706
1.00	.402	.402	.401	.50	1.723
1.50	.603	.603	.602	.75	1.743
2.00	.806	.806	.802	1.00	1.761
2.50	1.010	1.010	1.003	1.25	1.779
3.00	1.212	1.207	1.202	1.50	1.793
3.50	1.354	1.333	1.325	1.75	1.803
4.00	--	--	1.387	2.00	1.804
4.05	1.406	1.372	--	5.687	1.807
4.50	--	--	1.416	--	--
5.00	--	--	1.420	--	--

Cowl	Spike	Spike tip position, θ_l, deg	Internal contraction
I	I_a	31.0	1.305
I	I_b	31.4	1.250
I	I_c	31.4	1.273

2926

CJ-3 back

TABLE II. - 40° To 70° SPIKE INLET, II

	Spike II_a	Spike II_b	Cowl	
Coordinates, in.				
x	y	y	x (internal)	y (internal)
0	0	0	0	1.600
.5	.183	.183	.200	1.669
1.00	.363	.363	.400	1.723
1.50	.545	.545	.600	1.760
2.00	.728	.728	.800	1.784
2.50	.956	.956	1.000	1.797
3.00	1.275	1.264	1.100	1.800
3.50	1.469	1.448	5.600	1.800
4.00	1.541	1.514	--	--
4.40	1.550	1.520	--	--

Cowl	Spike	Spike tip position, θ_l, deg	Internal contraction
II	II_a	28.9	1.160
II	II_b	29.3	1.142

[redacted]

TABLE III. - ISENTROPIC SPIKE INLET WITH INTERNAL CONTRACTION, III

	Spike III_a	Spike III_b	Cowl	
Coordinates, in.				
x	y	y	x (internal)	y (internal)
0	0	0	0	1.500
.50	.136	.136	.169	1.573
1.00	.270	.270	.299	1.622
1.50	.405	.405	.499	1.687
2.00	.559	.559	.699	1.735
2.50	.752	.752	.899	1.771
3.00	1.037	1.023	1.099	1.792
3.50	1.370	1.352	1.299	1.800
4.00	1.554	1.523	5.205	1.800
4.50	1.613	1.573	--	--
4.60	1.615	1.574	--	--

Cowl	Spike	Spike tip position, θ_l, deg	Internal contraction
III	III_a	25.0	1.150
III	III_b	25.0	1.050

[redacted]

TABLE IV. - ISENTROPIC SPIKE INLET WITH NO INTERNAL CONTRACTION, IV

	Spike IV_a	Spike IV_b (porous)	Cowls IV_a and IV_b		Cowl IV_a	Cowl IV_b
	Coordinates, in.					
x	y	y	x	y (internal)	y (external)	y (external)
0	0	0	0	1.650	1.650	1.650
.50	.132	.120	.08	1.696	1.722	1.713
1.00	.265	.237	.18	1.732	1.811	1.762
1.50	.399	.358	.28	1.756	1.893	1.797
2.00	.544	.504	.38	1.772	1.948	1.821
2.50	.716	.664	.58	1.791	1.997	1.850
3.00	.941	.877	.78	1.798	2.000	1.861
3.50	1.298	1.182	1.00	1.800	--	1.862
3.75	1.491	1.418	5.63	1.800	--	--
4.00	1.535	1.534	--	--	--	--
4.50	1.547	1.547	--	--	--	--

Cowl	Spike	Spike tip position, θ_l, deg	Internal contraction
IV_a	IV_a	24.80	None
IV_a	IV_b	24.20	None
IV_b	IV_a	25.10	None

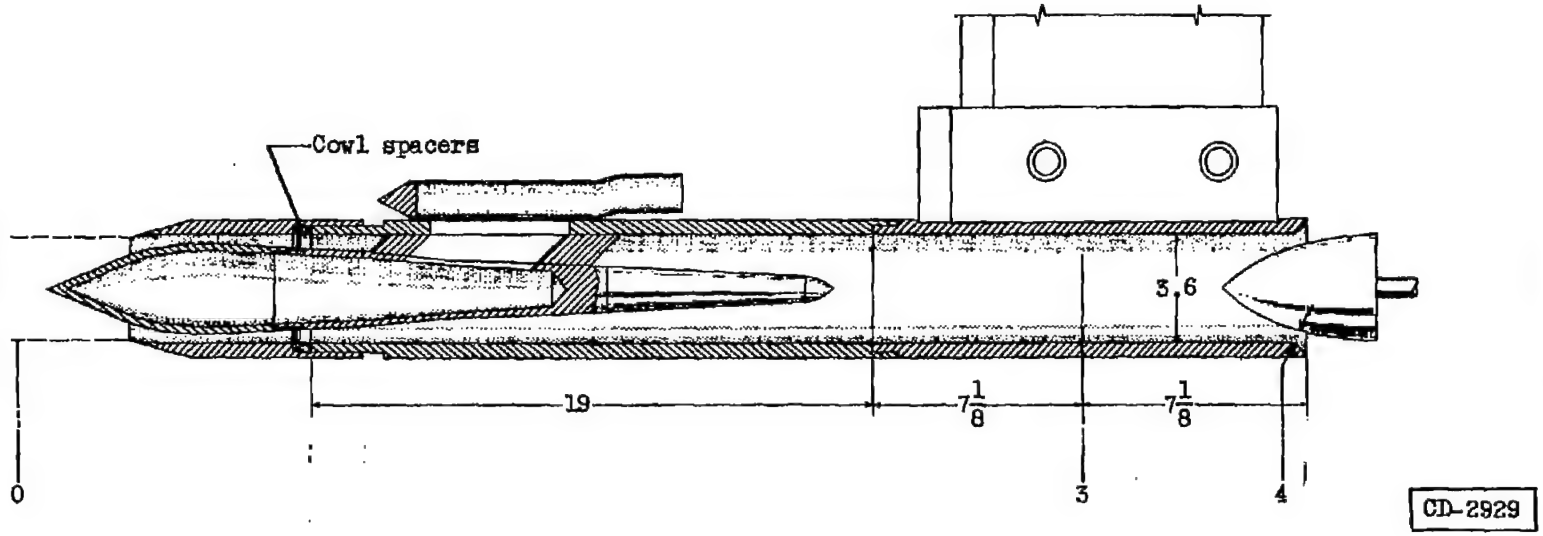

Figure 1. - Scale drawing of model arrangement with 1-cone inlet installed. (All dimensions in inches.)

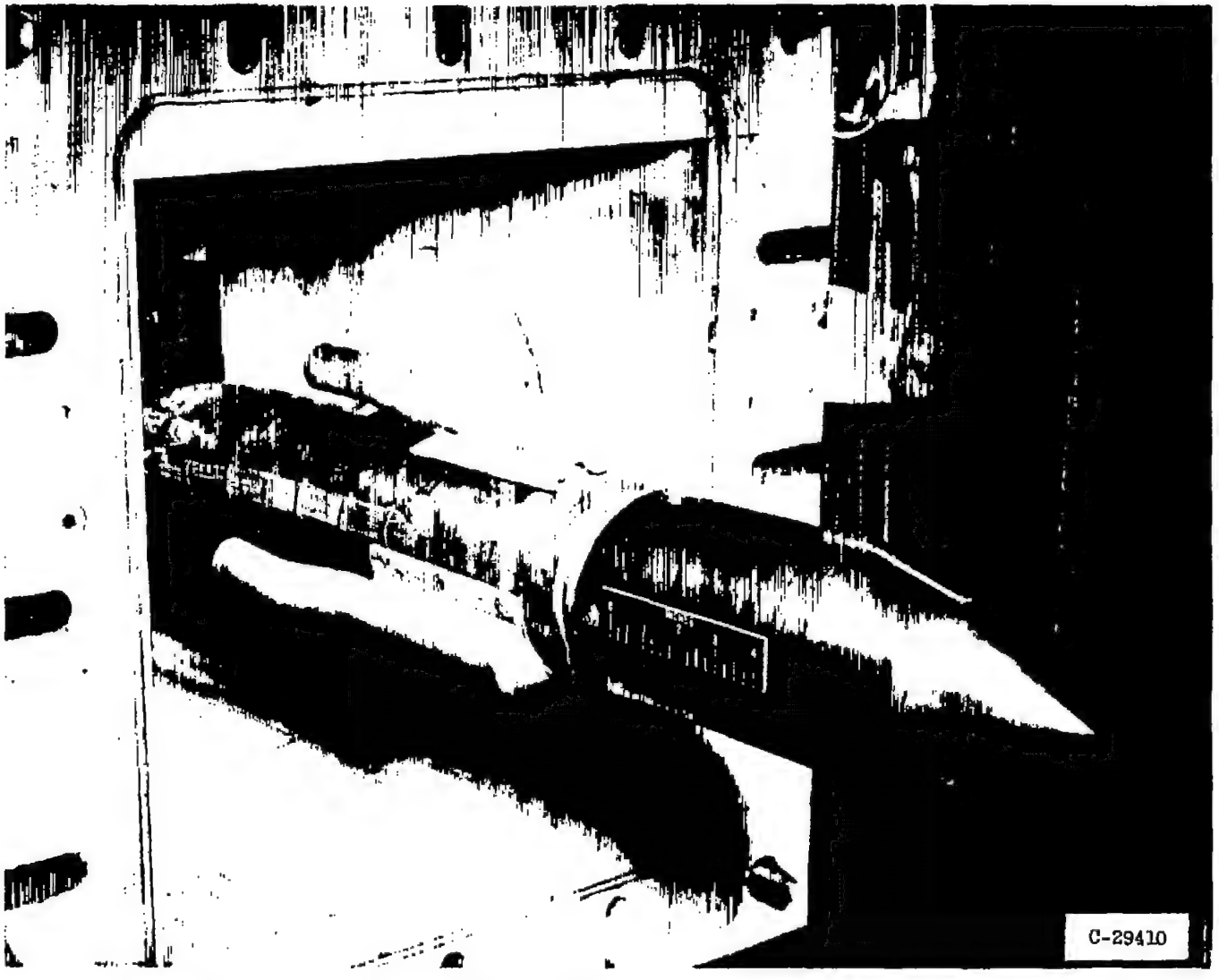

Figure 2. - Photograph of model mounted in tunnel. Inlet with cone-surface roughness.

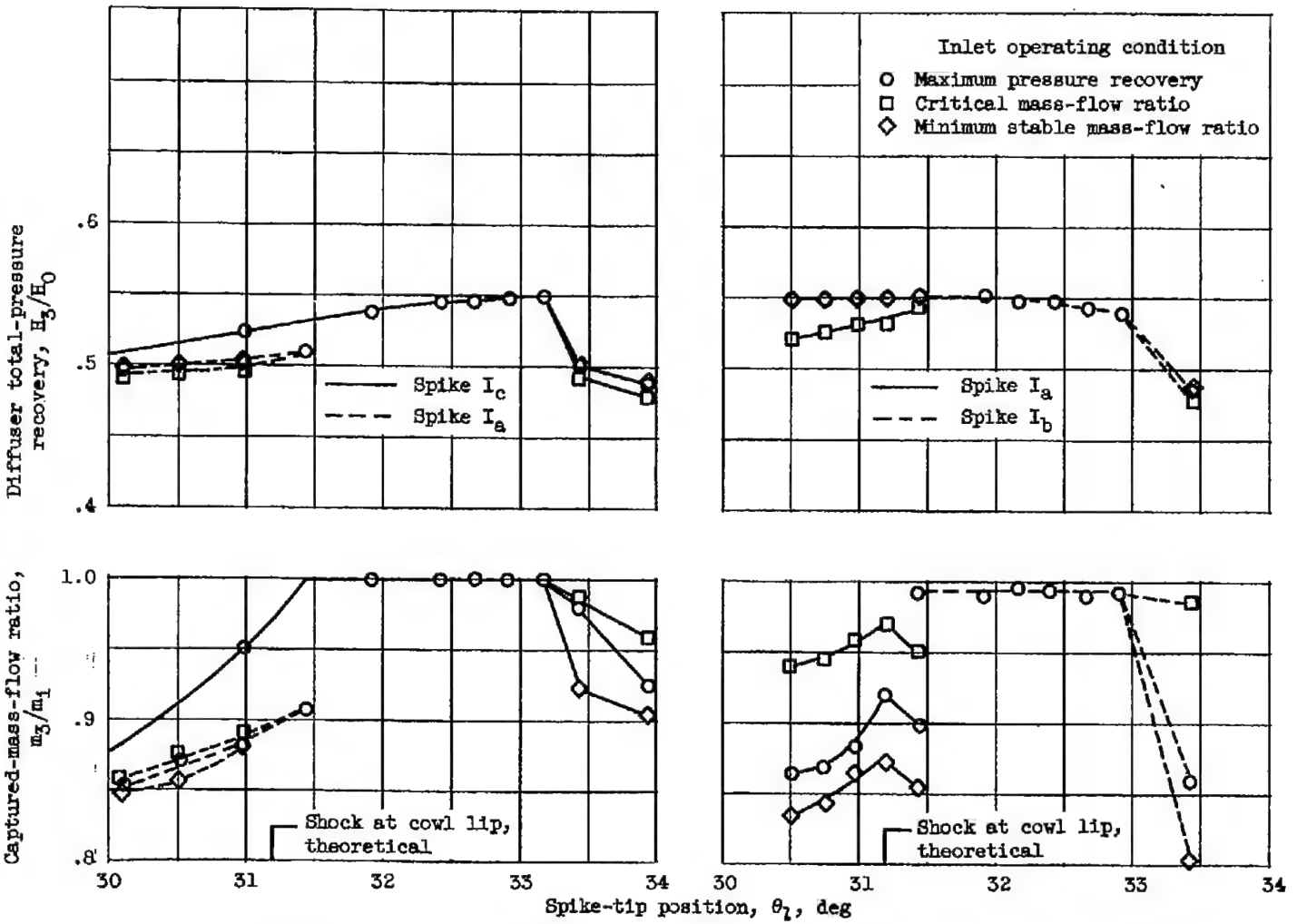

(a) Spikes I_a and I_c smooth.

(b) Spikes I_a and I_b with tip roughness.

Figure 3. - Comparison of three 44° 1-cone inlets. Free-stream Mach number, 3.05; Reynolds number, approximately 0.45×10^6; zero angle of attack.

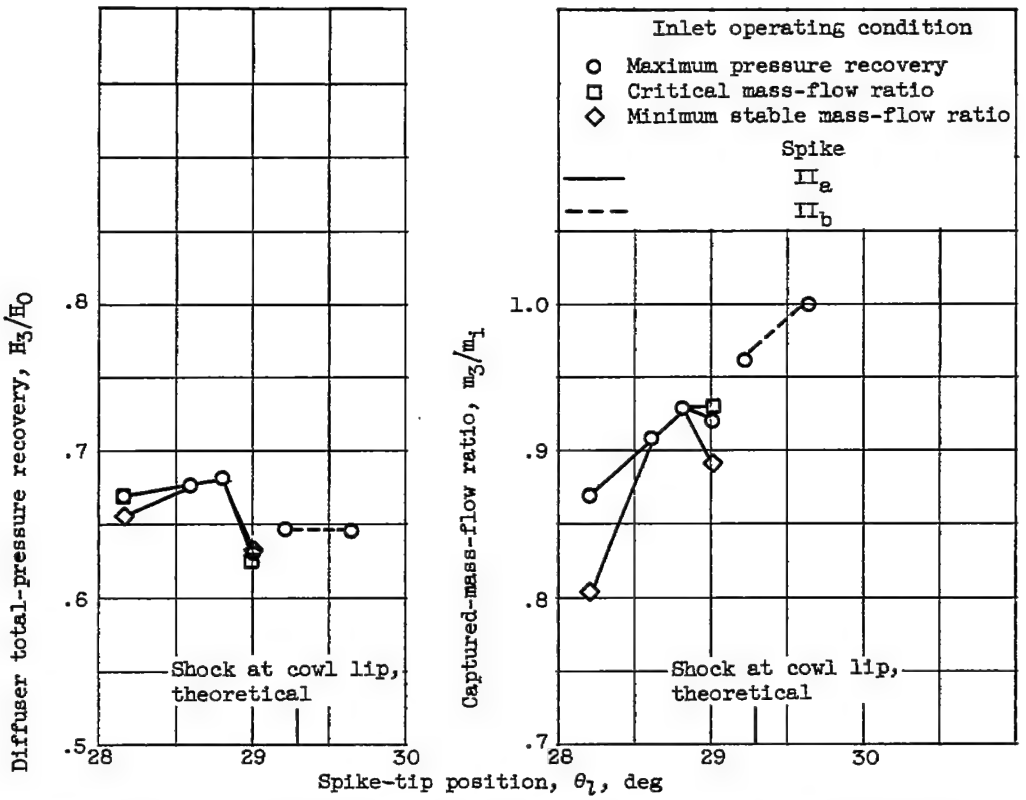

Figure 4. - Comparison of two 40° to 70° 2-cone inlets. Free-stream Mach number, 3.05; Reynolds number, approximately 0.45×10^6; zero angle of attack.

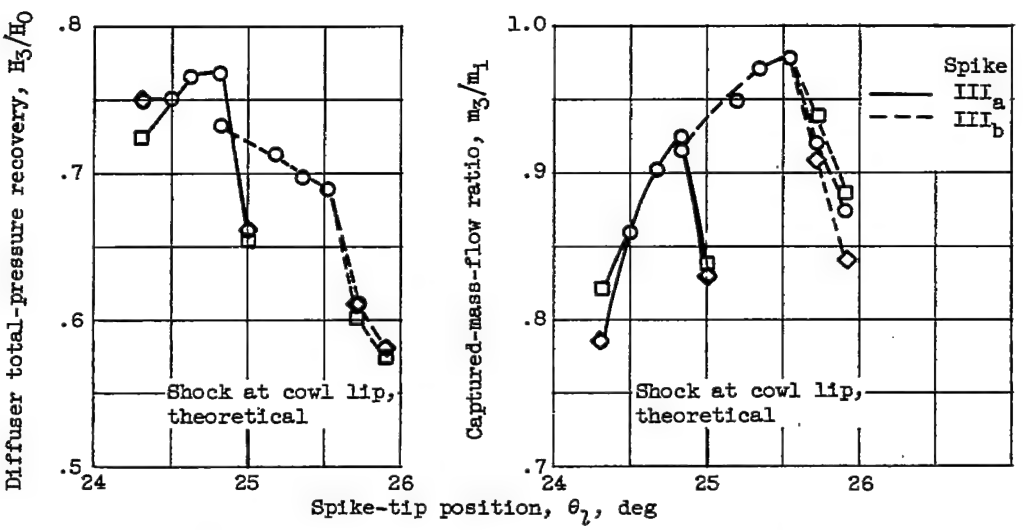

Figure 5. - Comparison of two isentropic inlets with internal contraction. Free-stream Mach number, 3.05; Reynolds number, approximately 0.45×10^6; zero angle of attack.

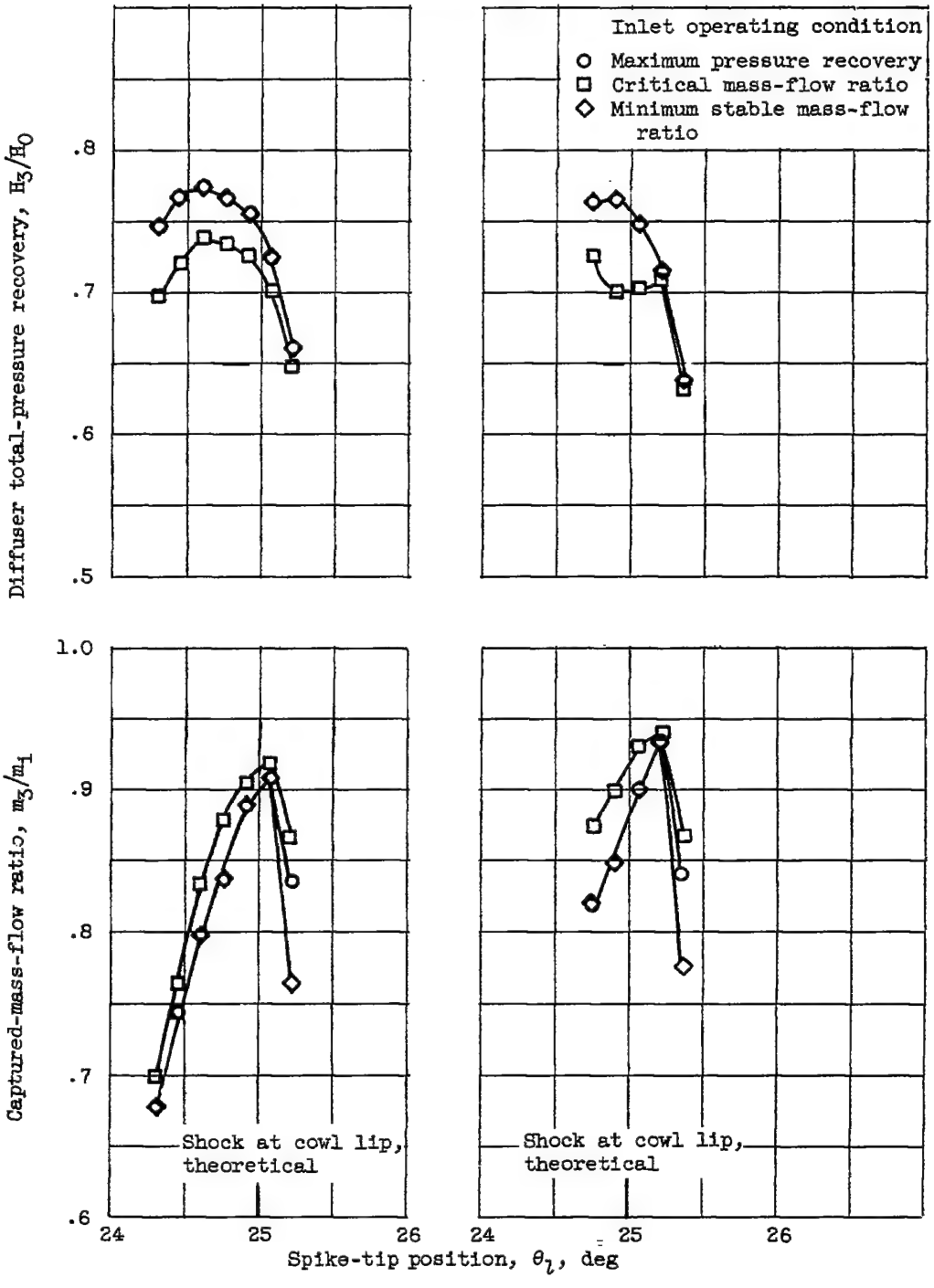

(a) Cowl IV_a. (b) Cowl IV_b.

Figure 6. - Performance of two isentropic inlets with no internal contraction. Spike IV_a; free-stream Mach number, 3.05; Reynolds number, approximately 0.45×10^6; zero angle of attack.

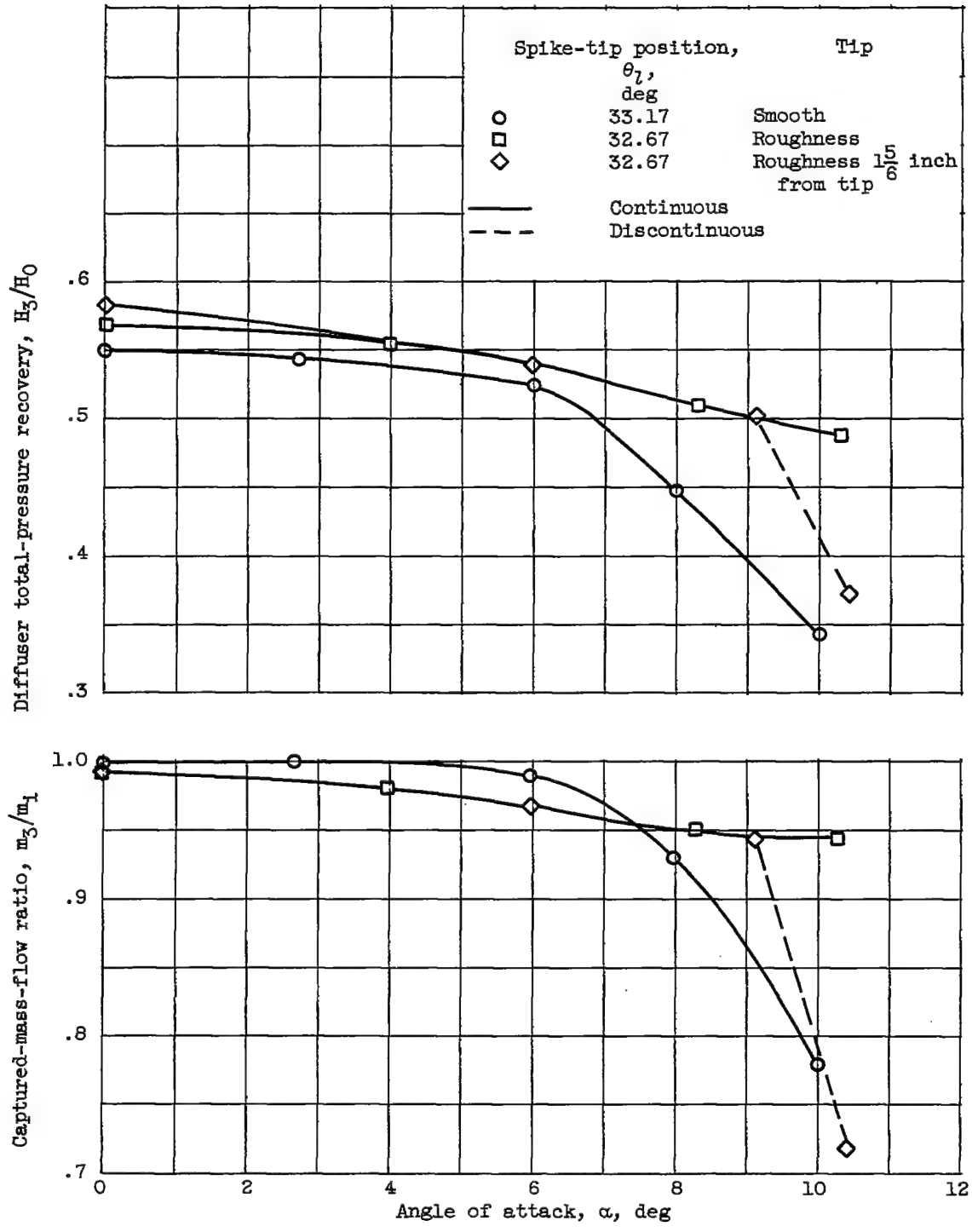

Figure 7. - Effect of angle of attack on peak pressure recovery of 44° 1-cone inlet. Spike I_c; free-stream Mach number, 3.05; Reynolds number, approximately 0.45×10^6.

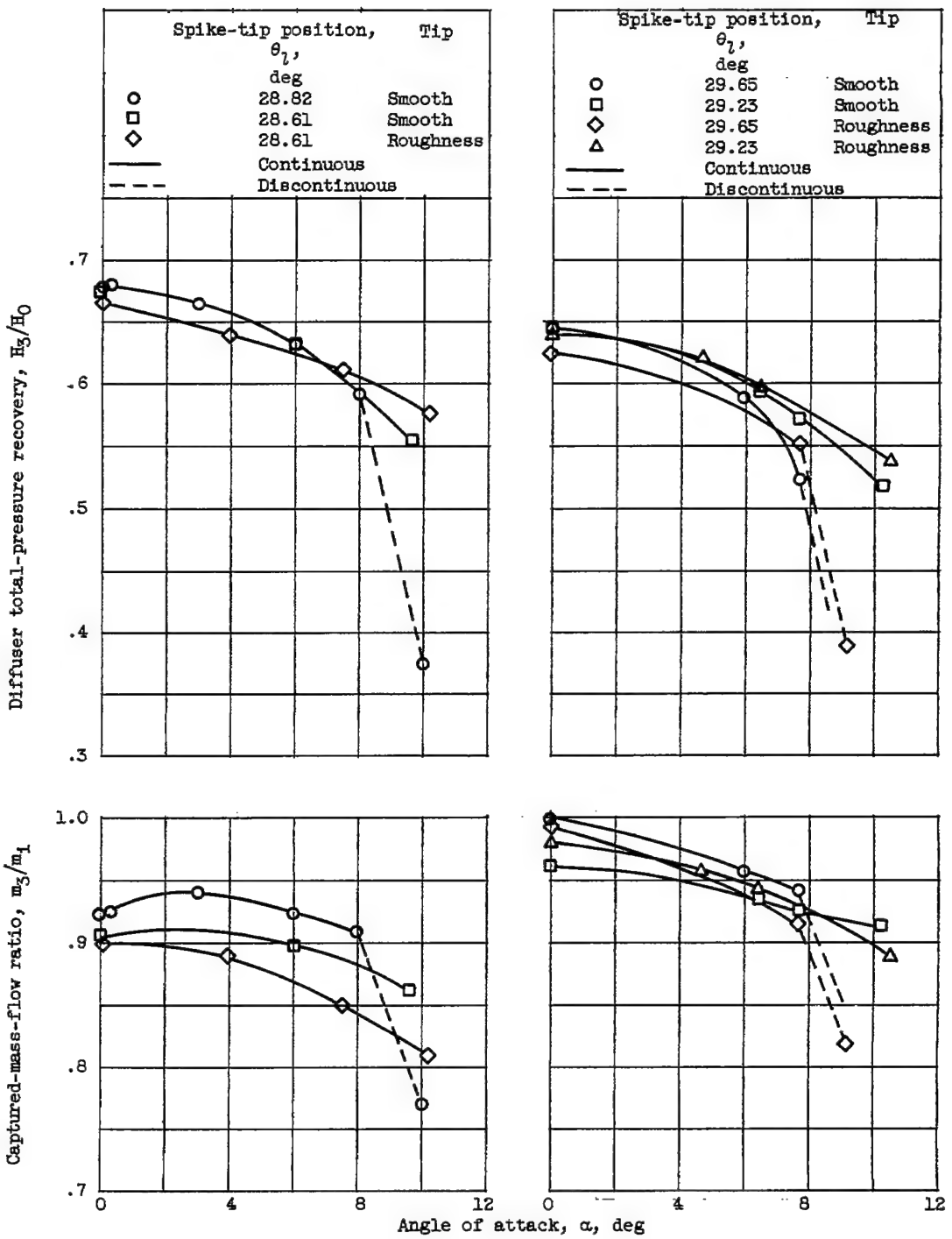

(a) Spike II_a. (b) Spike II_b.

Figure 8. - Effect of angle of attack on performance of two 40° to 70° 2-cone inlets. Free-stream Mach number, 3.05; Reynolds number, approximately 0.45×10^6.

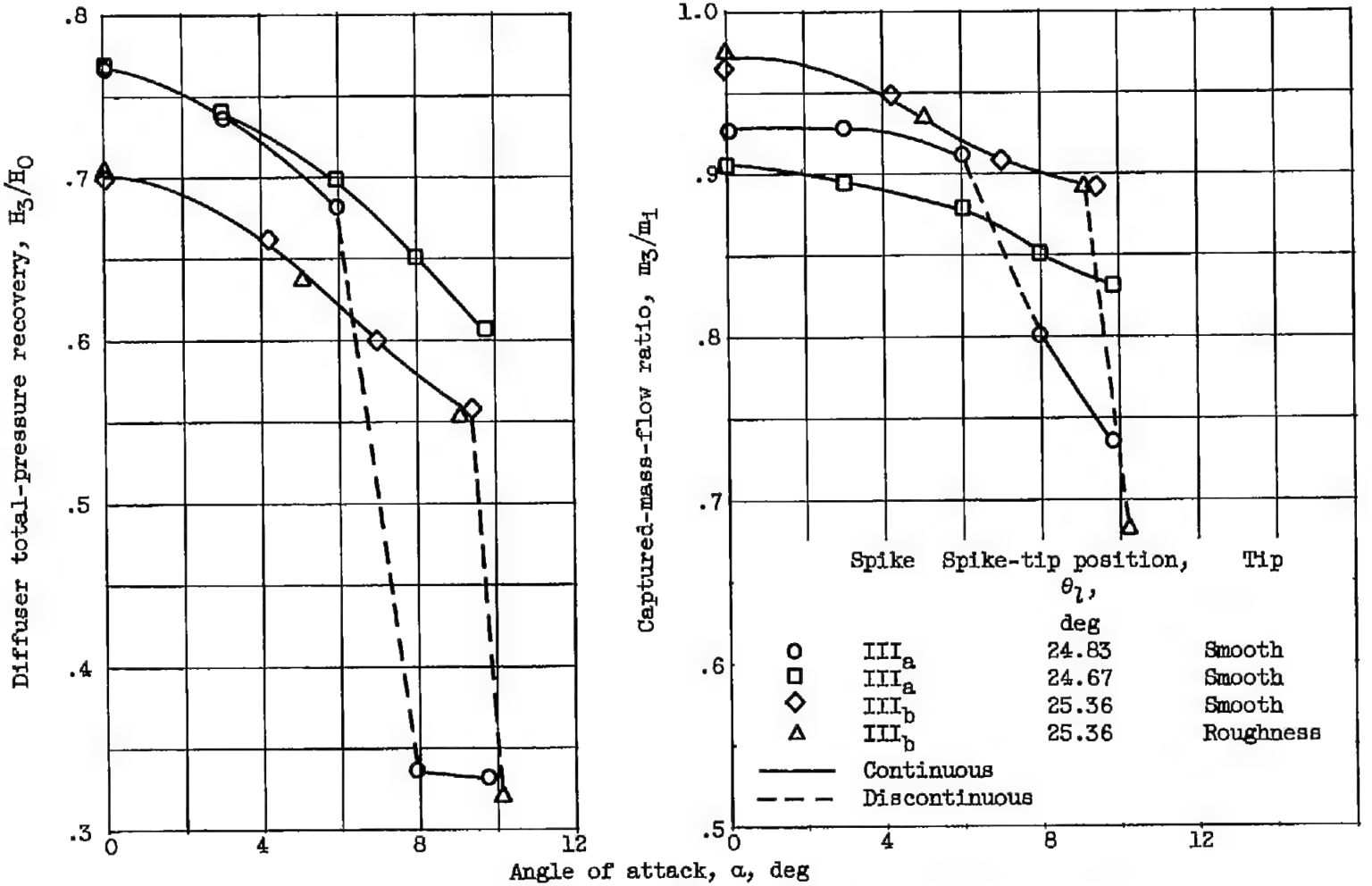

Figure 9. - Effect of angle of attack on performance of two isentropic inlets with internal contraction. Free-stream Mach number, 3.05; Reynolds number, approximately 0.45×10^6.

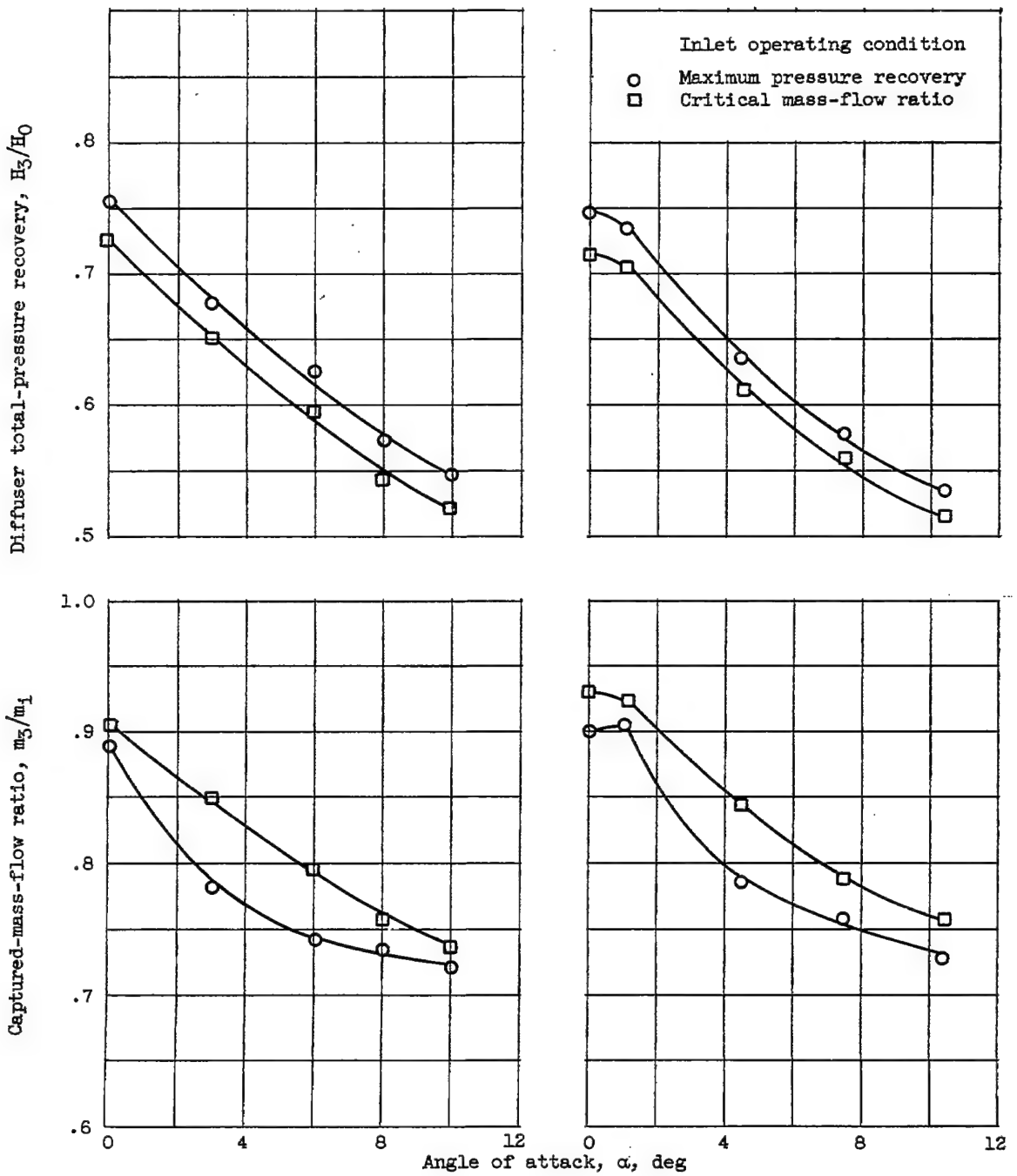

(a) Cowl IV_a; spike-tip position, 24.91°. (b) Cowl IV_b; spike-tip position, 25.07°.

Figure 10. - Effect of angle of attack on performance of two isentropic inlets with no internal contraction. Spike IV_a; free-stream Mach number, 3.05; Reynolds number, approximately 0.45×10^6.

[redacted]

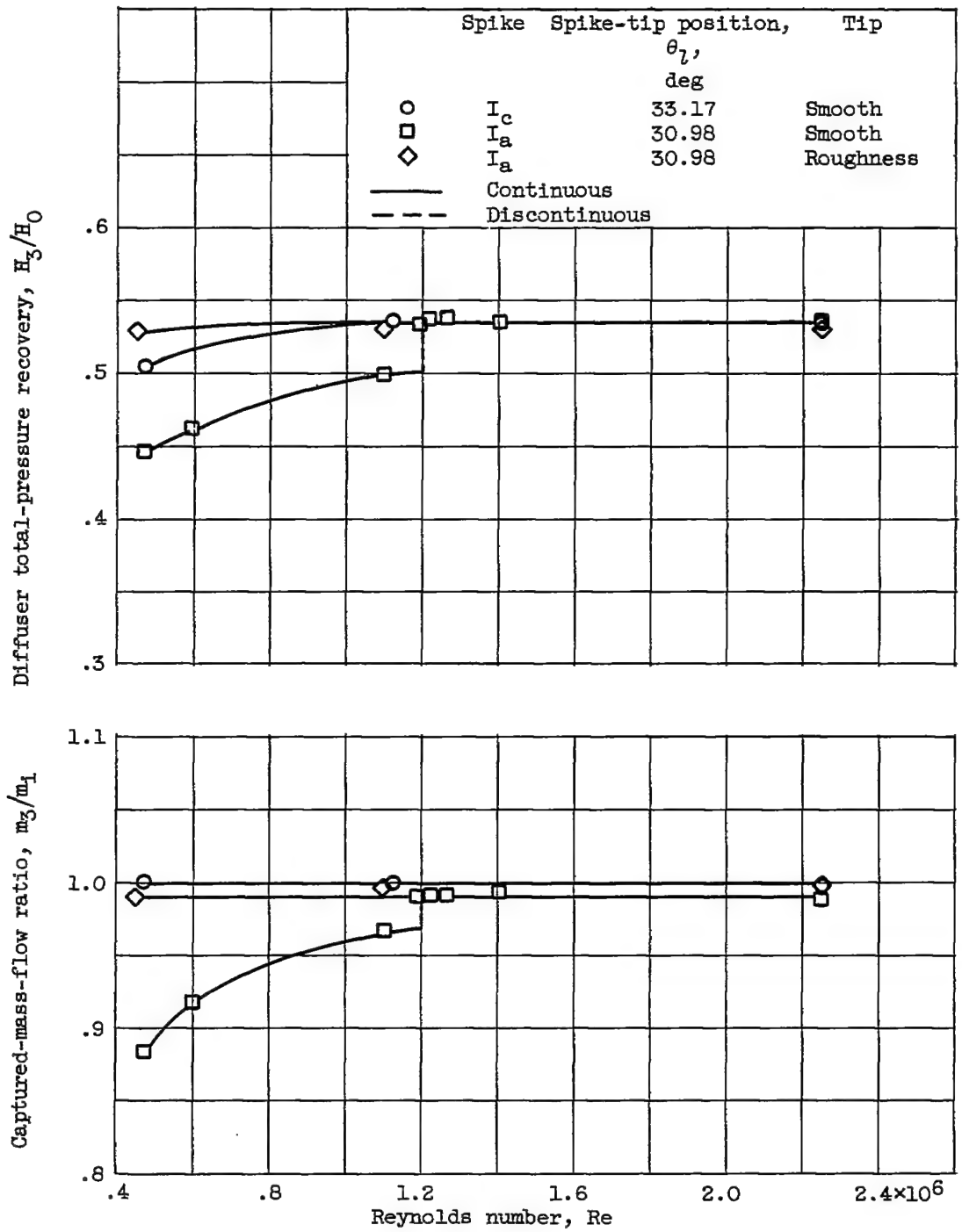

(a) Zero angle of attack.

Figure 11. - Effect of angle of attack on performance of 44° 1-cone inlet. Free-stream Mach number, 3.13.

[redacted]

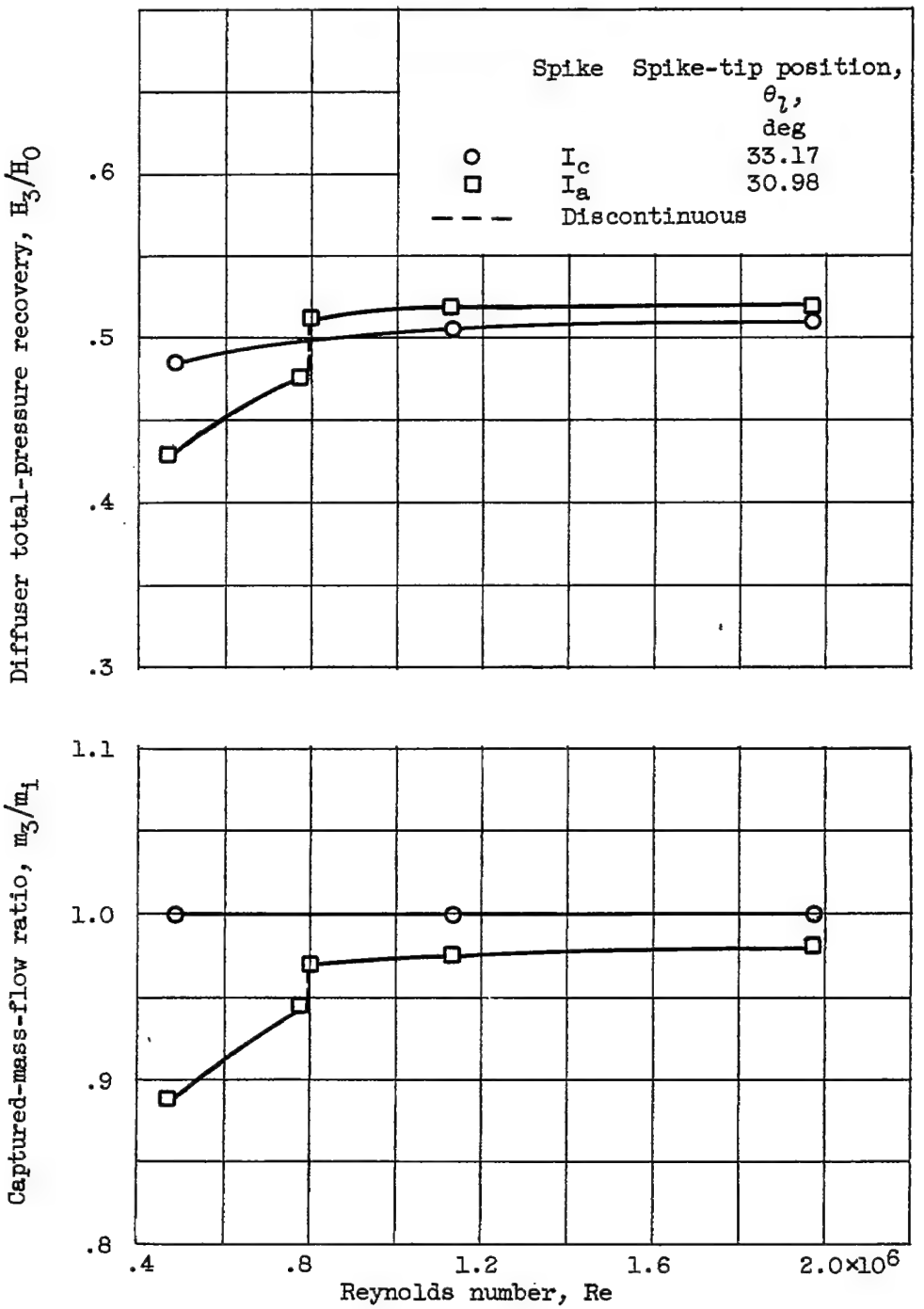

(b) Angle of attack, 4.9°.

Figure 11. - Concluded. Effect of angle of attack on performance of 44° 1-cone inlet. Free-stream Mach number, 3.13.

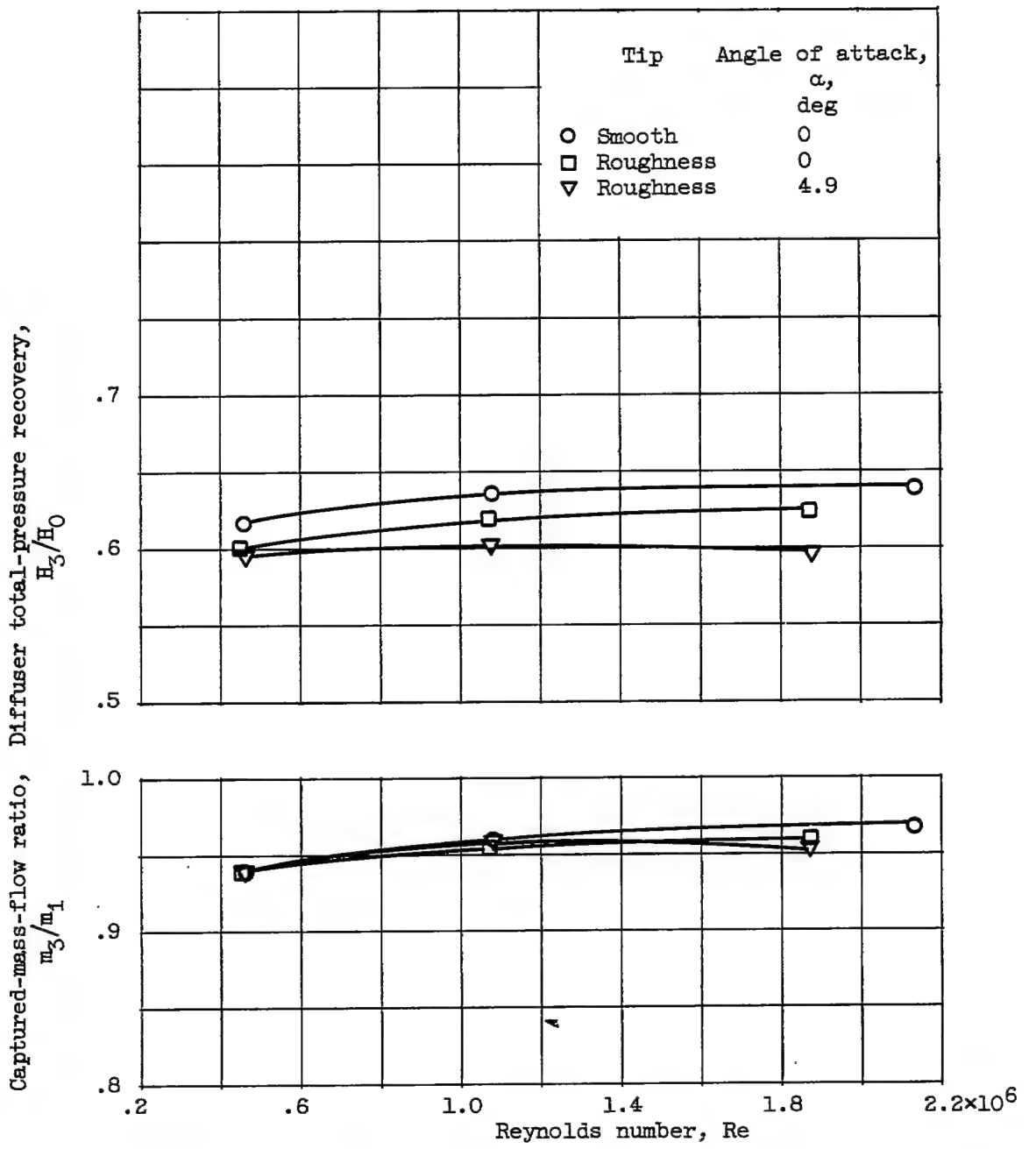

Figure 12. - Effect of Reynolds number on performance of 40° to 70° 2-cone inlet. Spike II_a; spike-tip position, 28.82°; free-stream Mach number, 3.13.

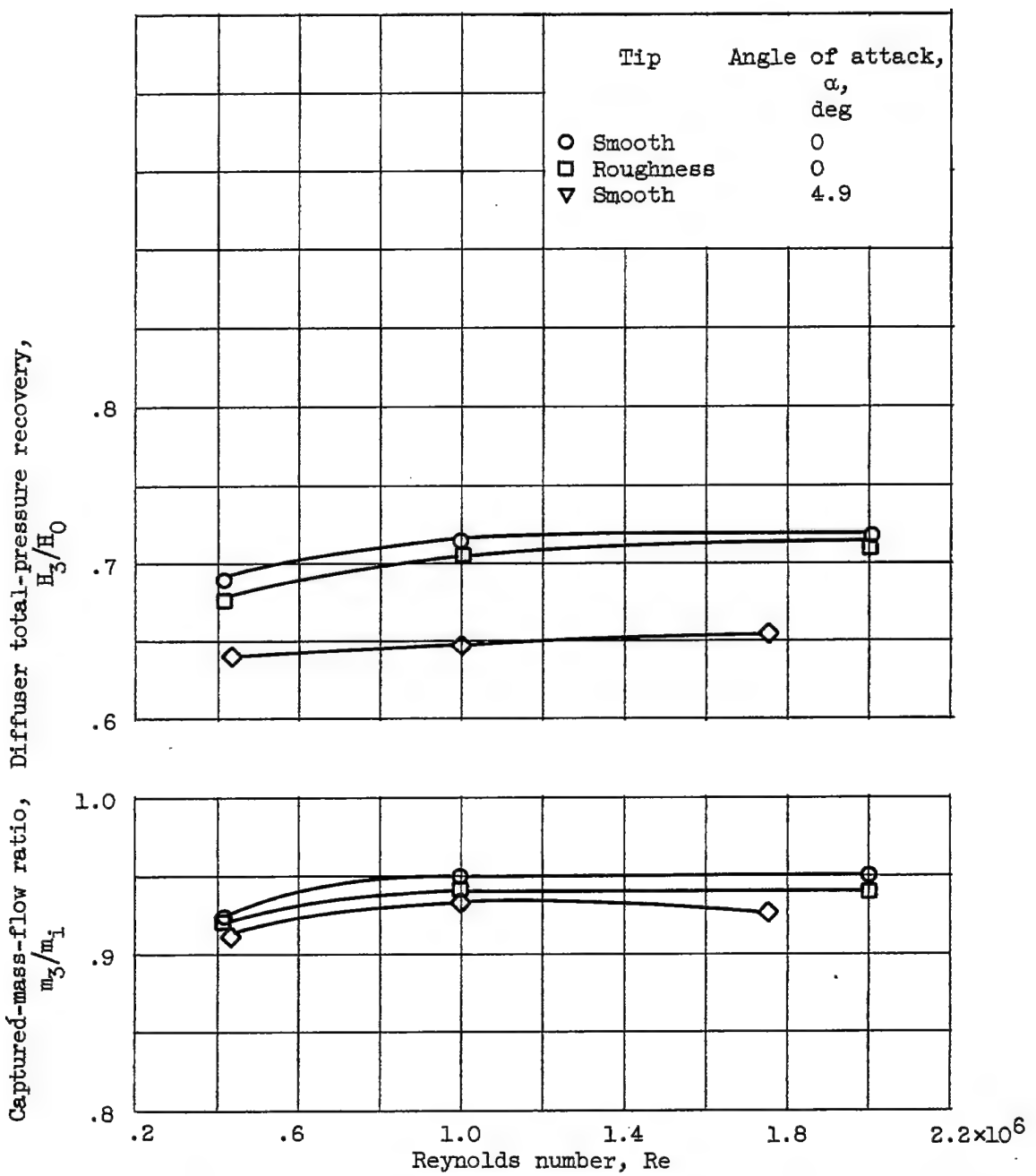

Figure 13. - Effect of Reynolds number on performance of isentropic inlet with internal contraction. Spike III_a; spike-tip position, 24.83°; free-stream Mach number, 3.13.

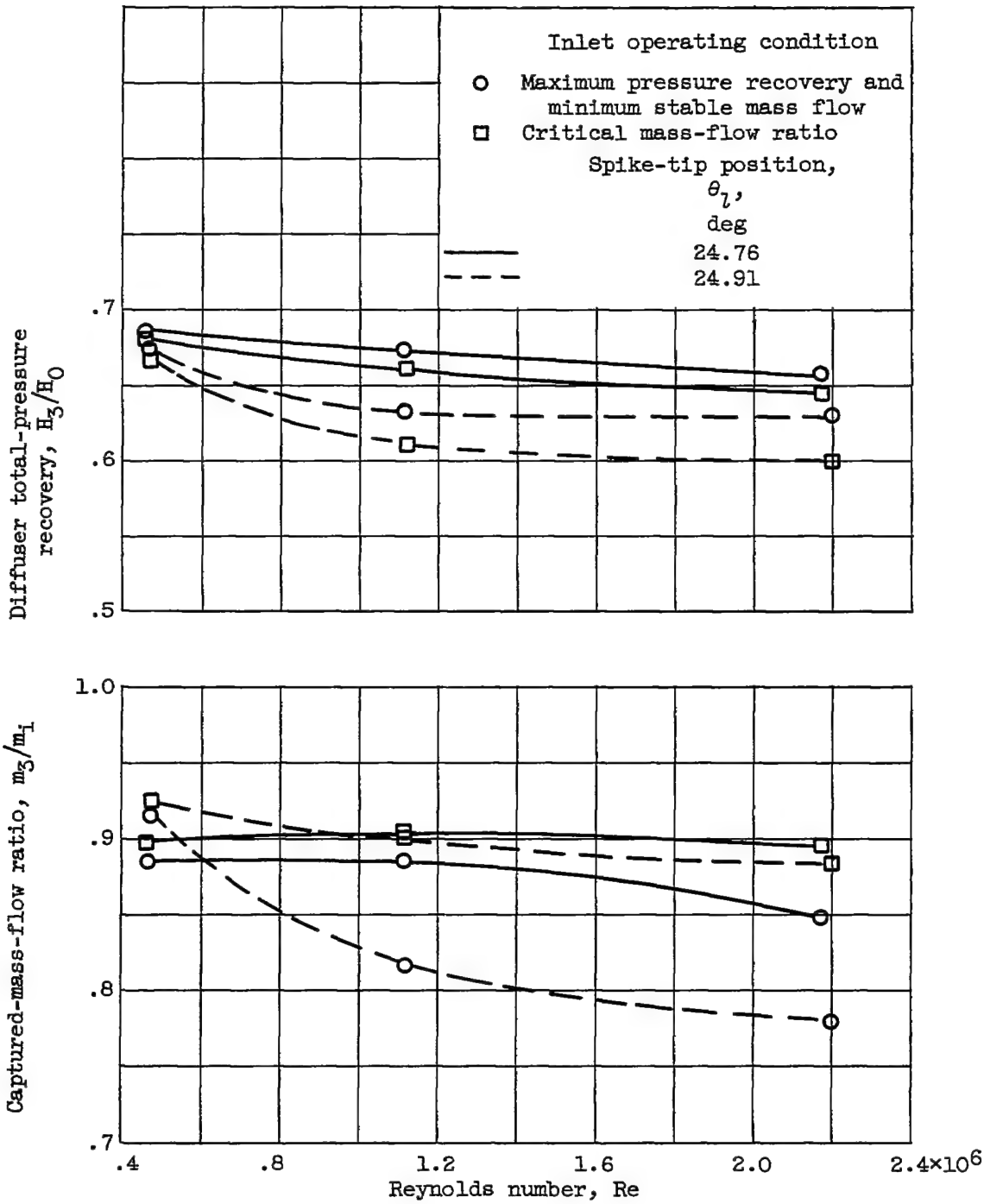

(a) Zero angle of attack.

Figure 14. - Effect of Reynolds number on performance of isentropic inlet with no internal contraction. Cowl IV_a; spike IV_a; free-stream Mach number, 3.13.

[redacted]

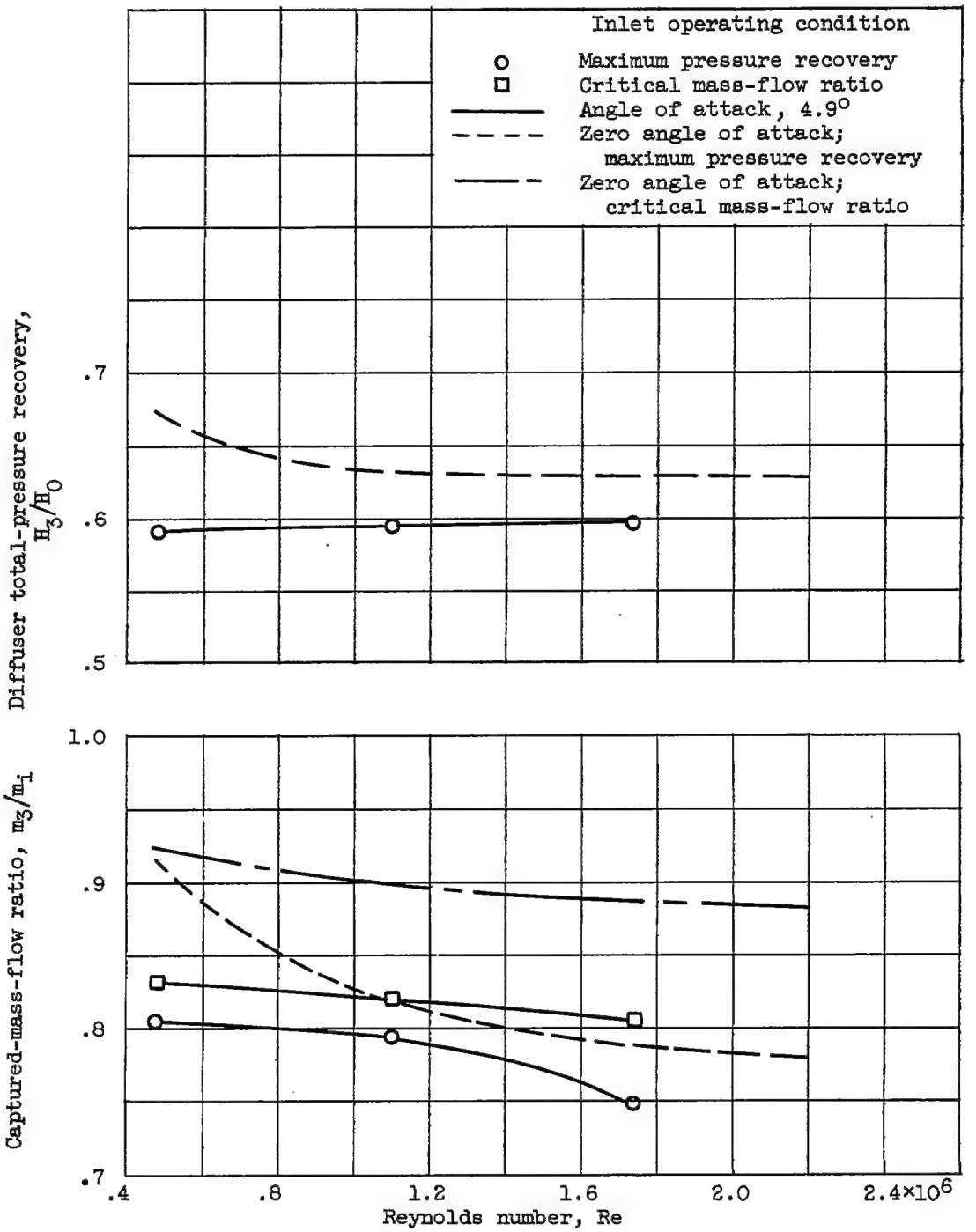

(b) Angle of attack, 4.9°; spike-tip position, 24.91°.

Figure 14. - Concluded. Effect of Reynolds number on performance of isentropic inlet with no internal contraction. Cowl IV_a; spike IV_a; free-stream Mach number, 3.13.

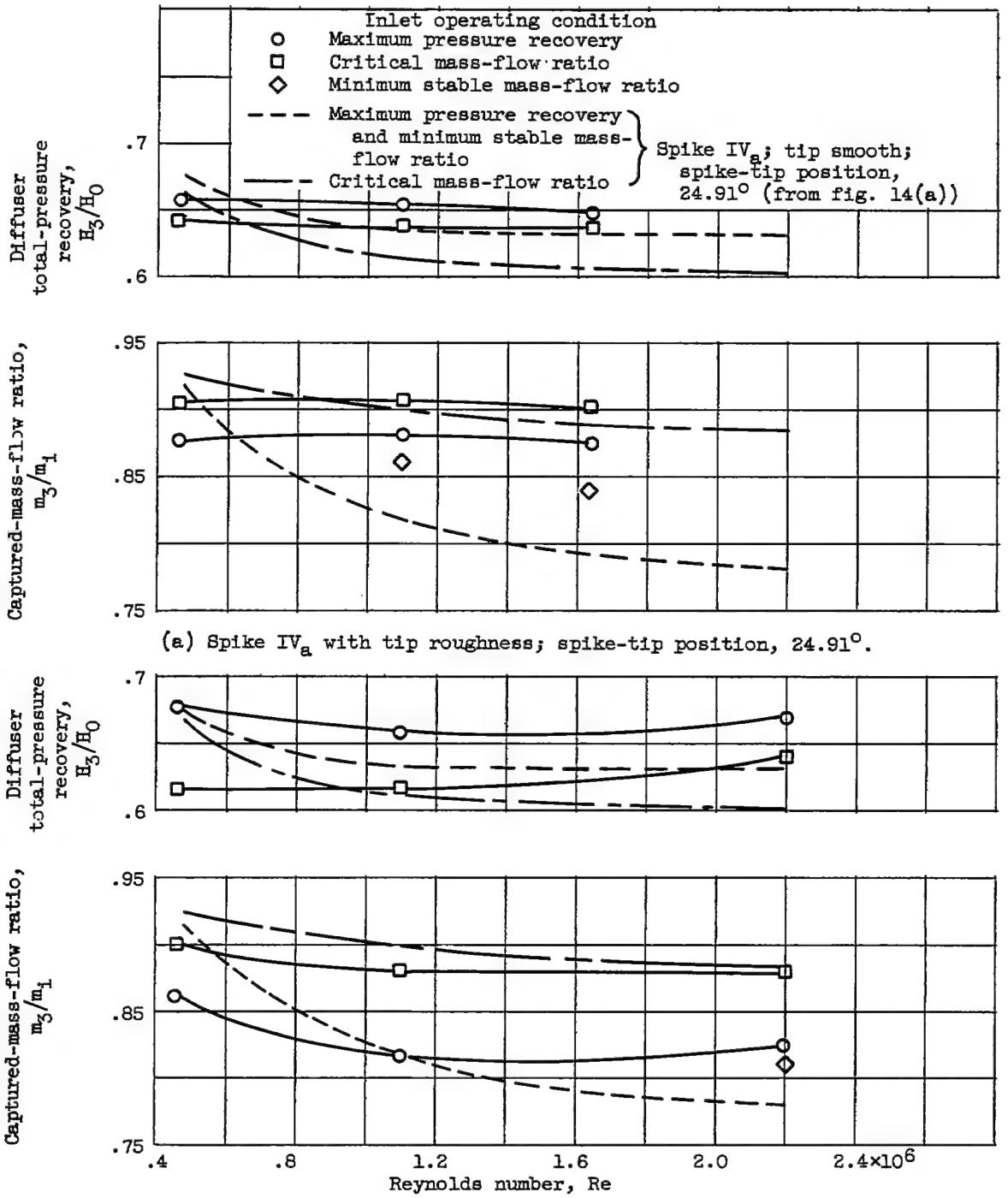

(a) Spike IV_a with tip roughness; spike-tip position, 24.91°.

(b) Spike IV_b (porous); spike-tip position, 24.33°.

Figure 15. - Effect of Reynolds number on performance of isentropic inlets with no internal contraction. Cowl IV_a; free-stream Mach number, 3.13; zero angle of attack.

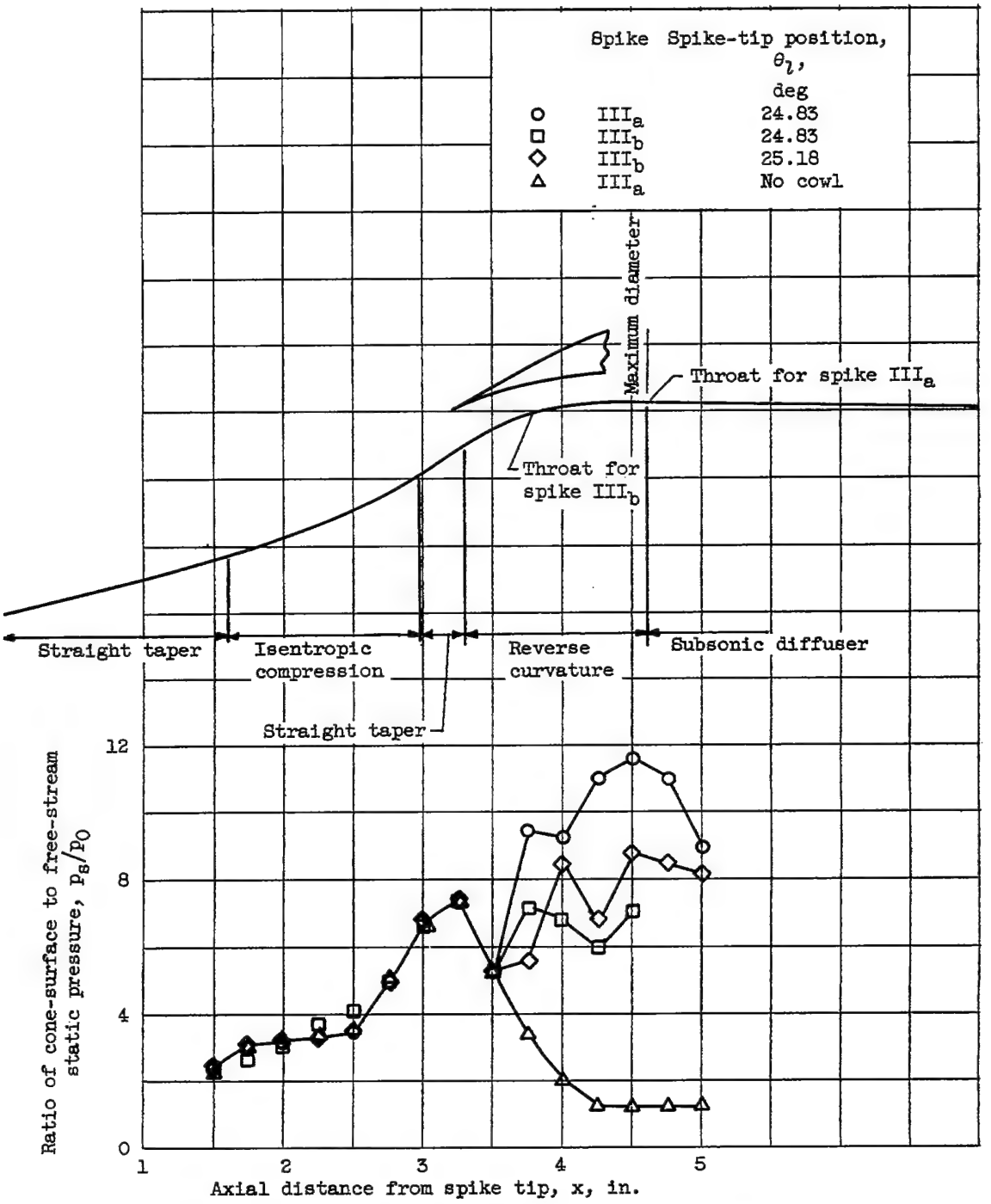

(a) Pressure recovery, approximately 0.53.

Figure 16. - Static-pressure distribution along centerbody of isentropic inlet with internal contraction. Free-stream Mach number, 3.05; Reynolds number, approximately 0.45×10^6; zero angle of attack.

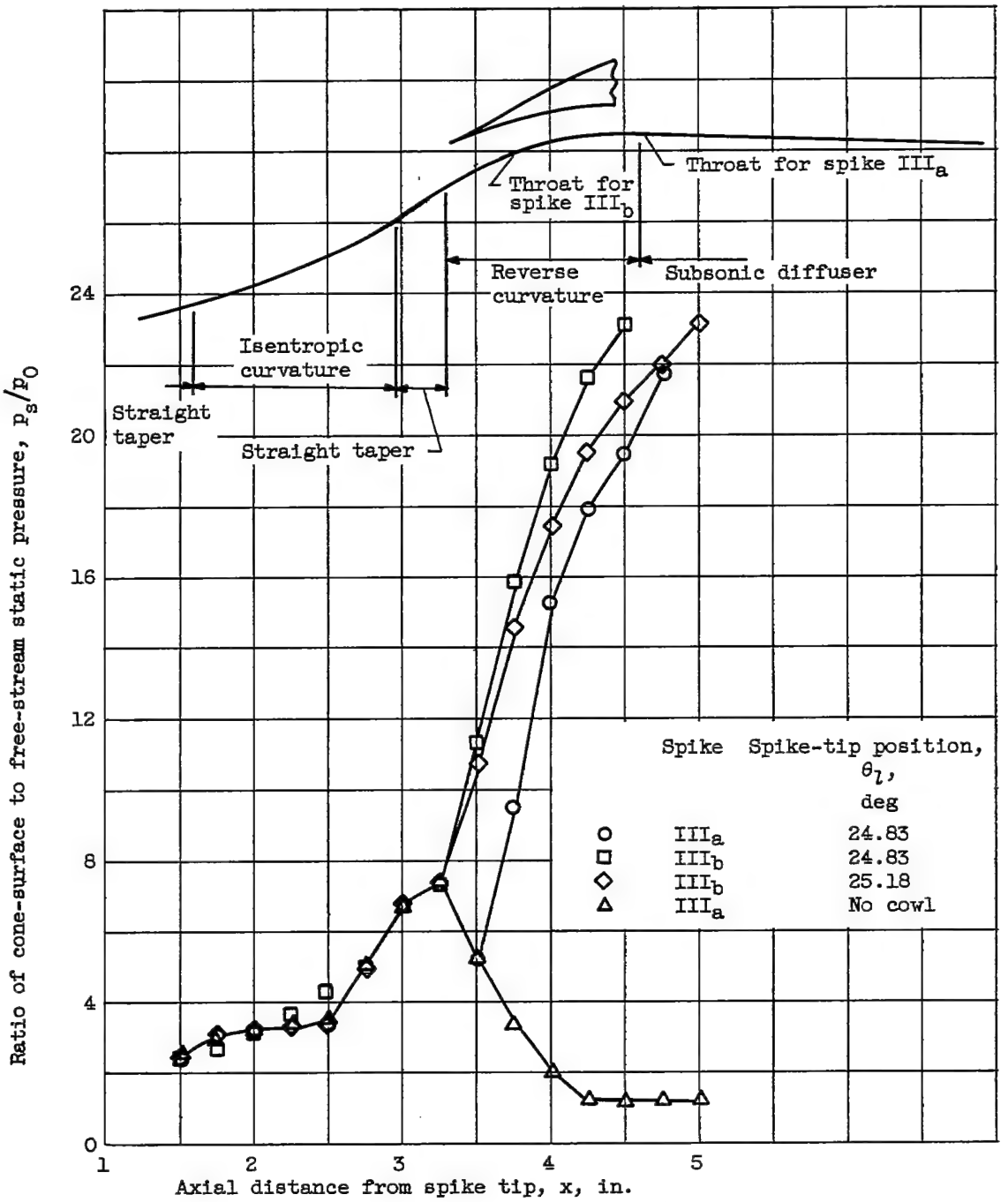

(b) Peak pressure recovery.

Figure 16. - Concluded. Static-pressure distribution along centerbody of isentropic inlet with internal contraction. Free-stream Mach number, 3.05; Reynolds number, approximately 0.45×10^6; zero angle of attack.

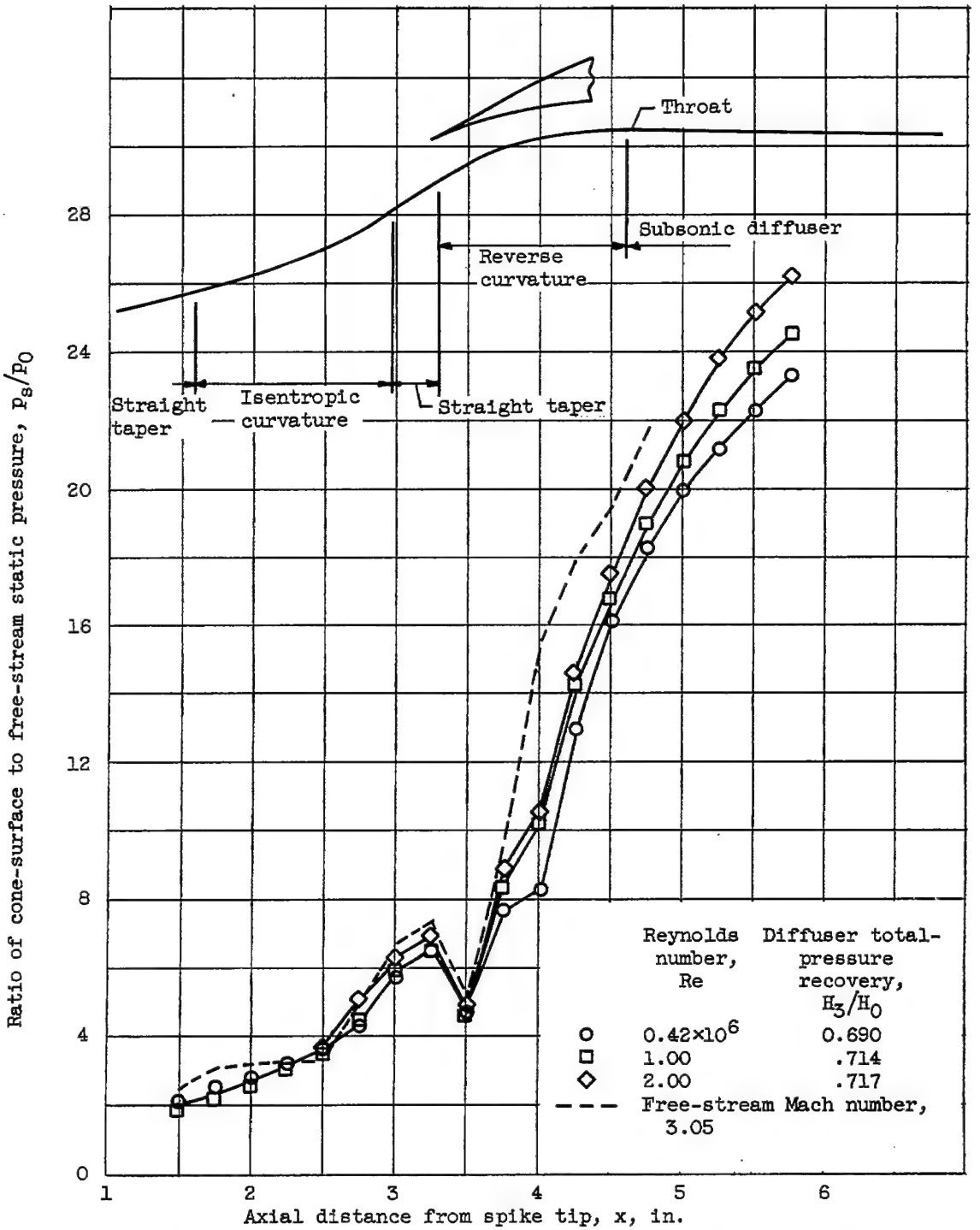

Figure 17. - Static-pressure distribution along centerbody of isentropic inlet with internal contraction at peak pressure recovery. Spike III_a; spike-tip position, 24.83°; free-stream Mach number, 3.13; zero angle of attack.

[redacted]

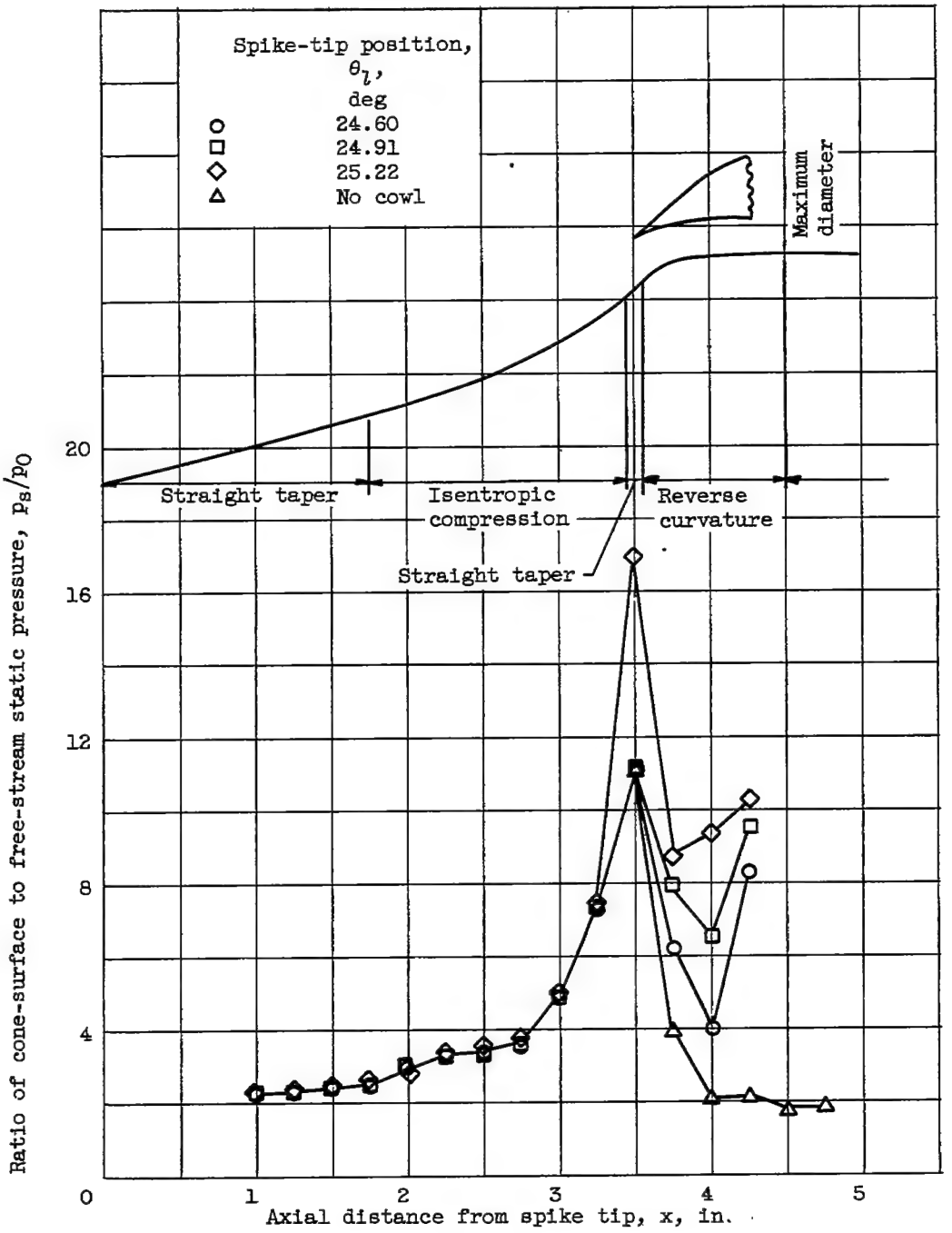

(a) Supercritical pressure recovery.

Figure 18. - Static-pressure distribution along centerbody of isentropic inlet with no internal contraction. Cowl IV_a; spike IV_a; free-stream Mach number, 3.05; Reynolds number, approximately 0.45×10^6; zero angle of attack.

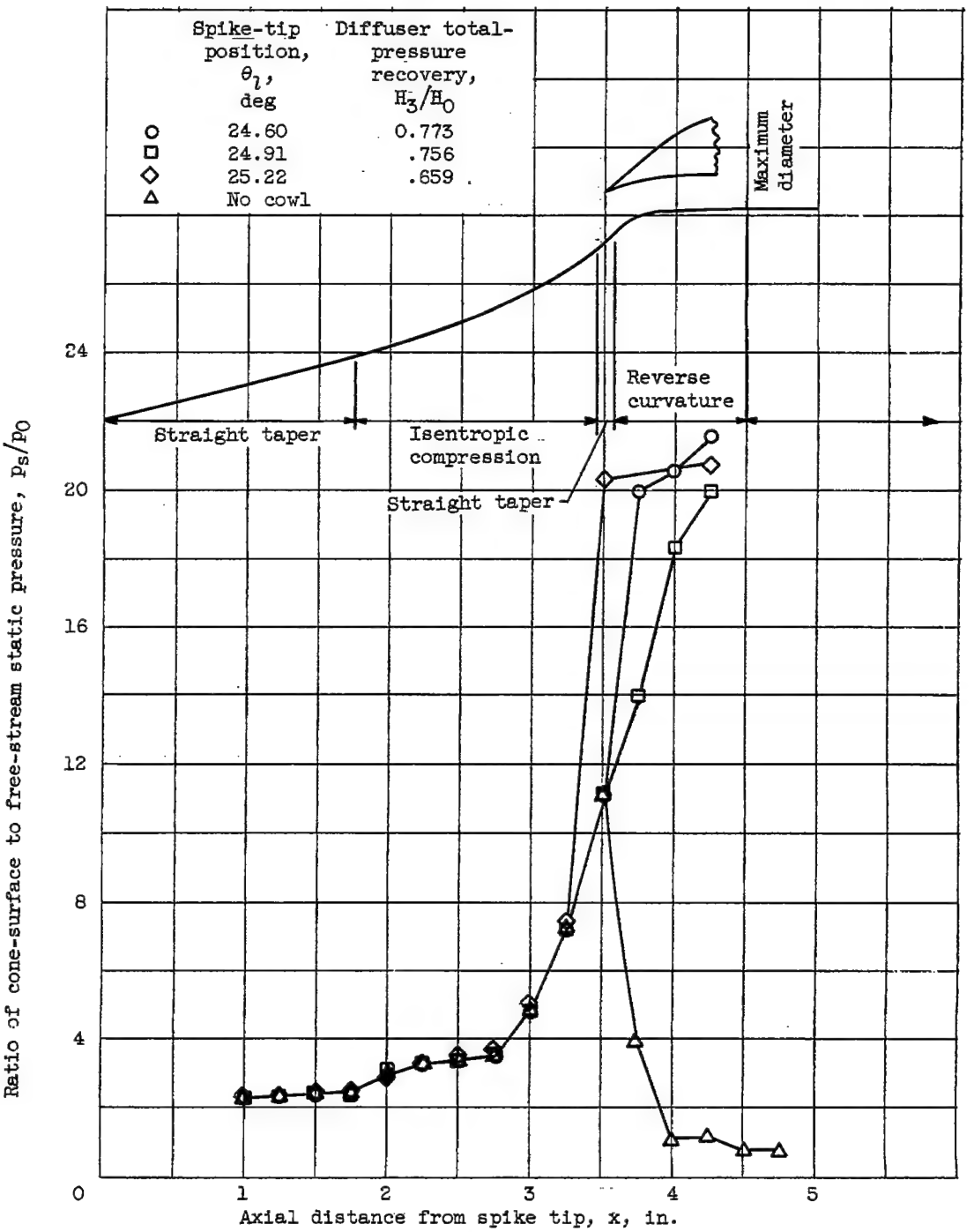

(b) Peak pressure recovery.

Figure 18. - Concluded. Static-pressure distribution along centerbody of isentropic inlet with no internal contraction. Cowl IV_a; spike IV_a; free-stream Mach number, 3.05; Reynolds number, approximately 0.45×10^6; zero angle of attack.

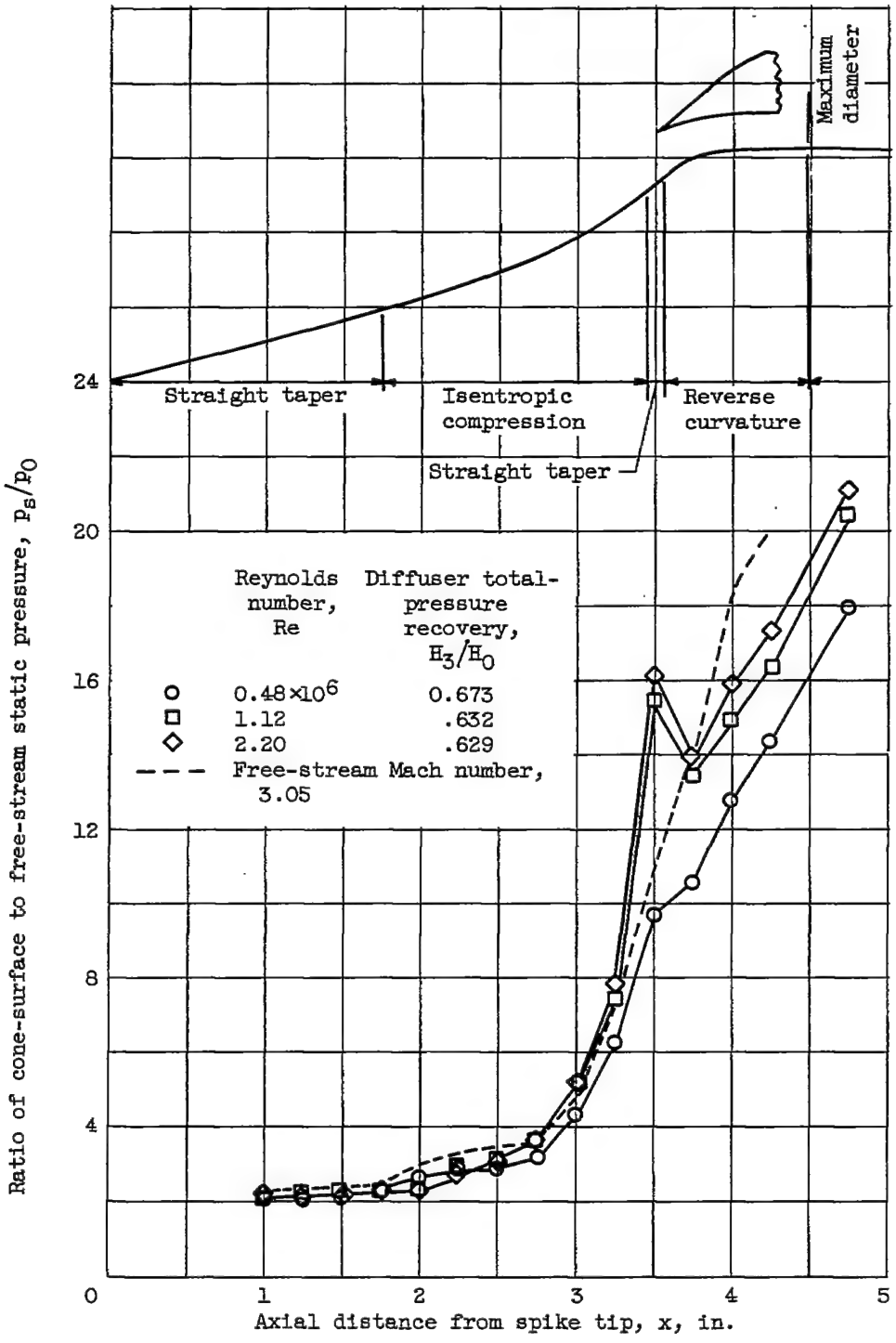

Figure 19. - Static-pressure distribution along centerbody of isentropic inlet with no internal contraction. Cowl IV_a; spike IV_a; spike-tip position, 24.91°; free-stream Mach number, 3.13; zero angle of attack.

(a) Spike I_c; no cowl; free-stream Mach number, 3.05; Reynolds number, 0.45×10^6.

(b) Spike I_c; spike-tip position, 32.92°; free-stream Mach number, 3.05; Reynolds number, 0.45×10^6; diffuser total-pressure recovery, 0.547; captured-mass-flow ratio, 1.0.

(c) Spike I_a; spike-tip position, 30.98°; free-stream Mach number, 3.05; Reynolds number, 0.45×10^6; diffuser total-pressure recovery, 0.465; captured-mass-flow ratio, 0.89.

(d) Spike I_a; spike-tip position, 30.98°; free-stream Mach number, 3.13; Reynolds number, 0.47×10^6; diffuser total-pressure recovery, 0.440; captured-mass-flow ratio, 0.88.

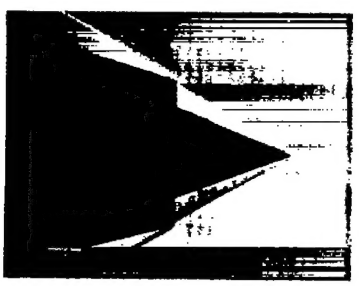

(e) Spike I_c with tip roughness; spike-tip position, 32.67°; free-stream Mach number, 3.05; Reynolds number, 0.45×10^6; diffuser total-pressure recovery, 0.498; captured-mass-flow ratio, 0.99.

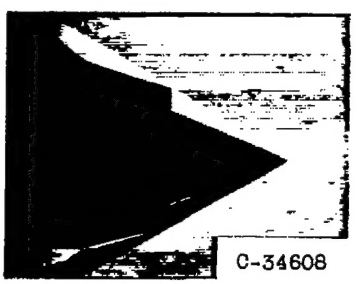

(f) Spike I_a; spike-tip position, 30.98°; free-stream Mach number, 3.13; Reynolds number, 1.26×10^6; diffuser total-pressure recovery, 0.418; captured-mass-flow ratio, 0.99.

Figure 20. - Schlieren photographs of 1-cone inlet at zero angle of attack with various boundary-layer conditions along cone surface.

(a) Angle of attack, 2.7°; spike-tip position, 33.17°; diffuser total-pressure recovery, 0.543; captured-mass-flow ratio, 1.00.

(b) Angle of attack, 6°; spike-tip position, 33.17°; diffuser total-pressure recovery, 0.516; captured-mass-flow ratio, 0.99.

(c) Angle of attack, 8°; spike-tip position, 33.17°; diffuser total-pressure recovery, 0.453; captured-mass-flow ratio, 0.94.

(d) Angle of attack, 10°; spike-tip position, 33.17°; diffuser total-pressure recovery, 0.347; captured-mass-flow ratio, 0.76.

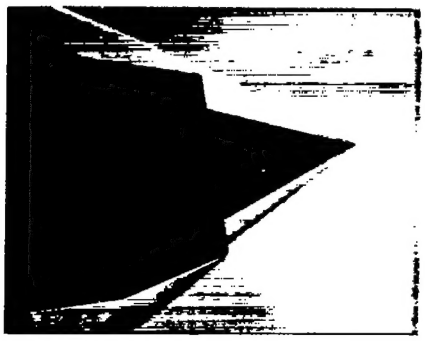

(e) Angle of attack, 8.3°; spike-tip position, 32.67°; tip roughness; diffuser total-pressure recovery, 0.510; captured-mass-flow ratio, 0.95.

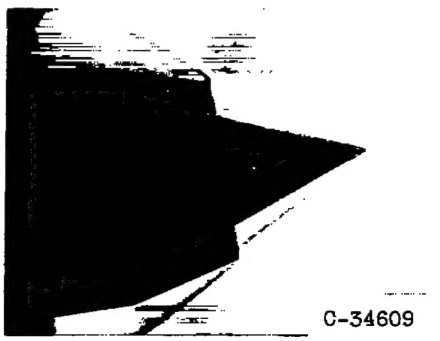

(f) Angle of attack, 10.3°; spike-tip position, 32.67°; tip roughness; diffuser total-pressure recovery, 0.487; captured-mass-flow ratio, 0.94.

Figure 21. - Schlieren photographs of 1-cone inlet at angle of attack. Spike I_o; free-stream Mach number, 3.05; Reynolds number, 0.45×10^6.

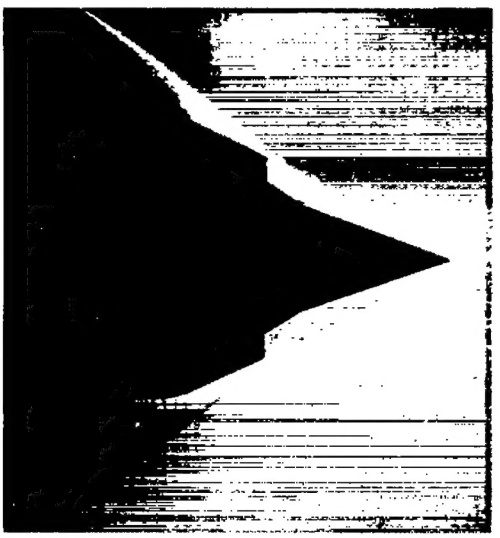

(a) Spike II_a; spike-tip position, 28.82°; free-stream Mach number, 3.13; Reynolds number, 0.45×10^6; zero angle of attack; diffuser total-pressure recovery, 0.389; captured-mass-flow ratio, 0.94.

(b) Spike II_a; spike-tip position, 28.82°; free-stream Mach number, 3.13; Reynolds number, 2.13×10^6; zero angle of attack; diffuser total-pressure recovery, 0.639; captured-mass-flow ratio, 0.97.

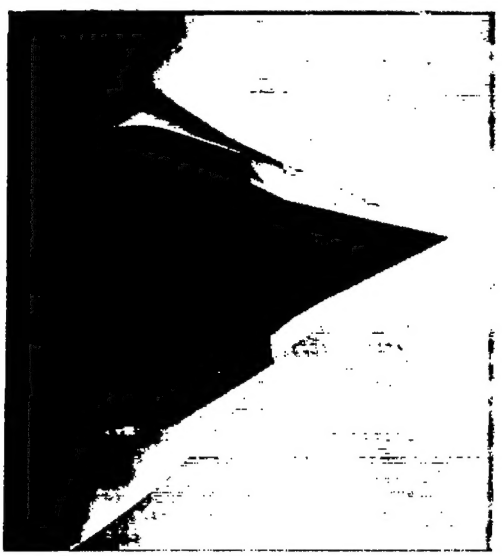

(c) Spike II_a; spike-tip position, 29.23°; free-stream Mach number, 3.05; Reynolds number, 0.45×10^6; angle of attack, 6.5°; diffuser total-pressure recovery, 0.596; captured-mass-flow ratio, 0.93.

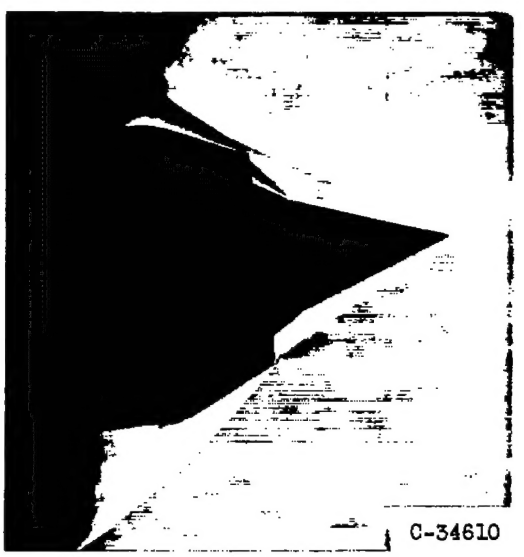

(d) Spike II_b with tip roughness; spike-tip position, 29.23°; free-stream Mach number, 3.05; Reynolds number, 0.45×10^6; angle of attack, 6.5°; diffuser total-pressure recovery, 0.599; captured-mass-flow ratio, 0.94.

Figure 22. - Schlieren photographs of 2-cone inlet.

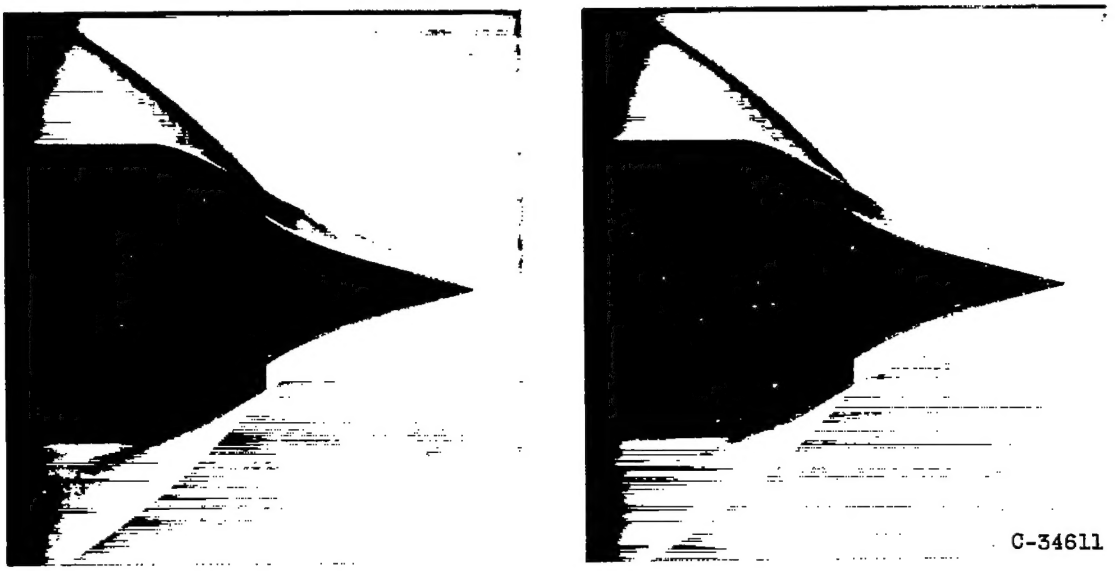

(a) Diffuser total-pressure recovery, 0.700; captured-mass-flow ratio, 0.96.

(b) Tip roughness; diffuser total-pressure recovery, 0.706; captured-mass-flow ratio, 0.97.

Figure 23. - Schlieren photographs of isentropic inlet with internal contraction. Spike III_b; spike-tip position, 25.36°; free-stream Mach number, 3.05; Reynolds number, 0.45×10^6; zero angle of attack.

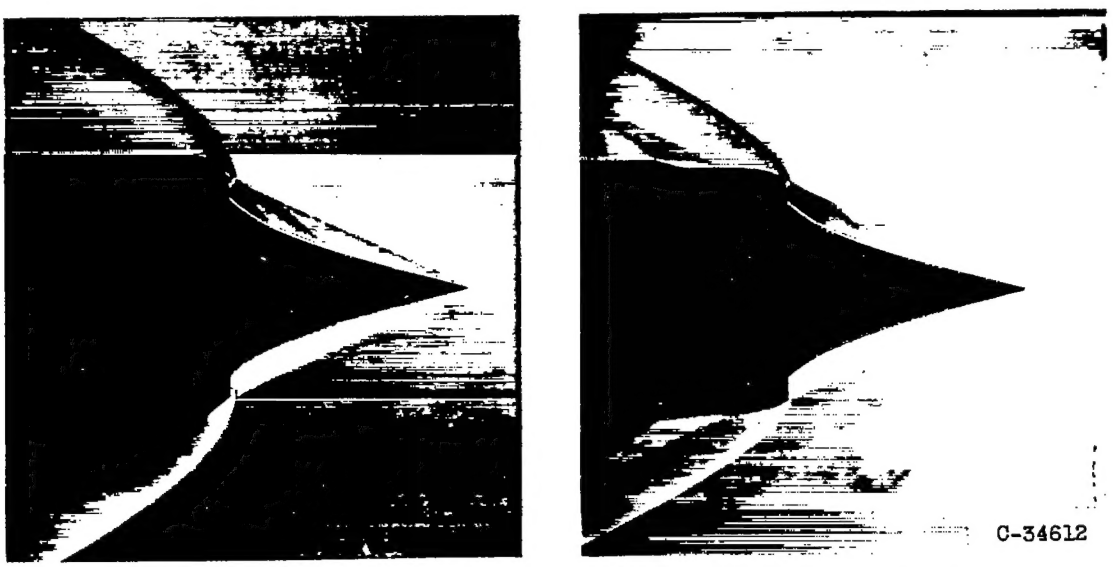

(a) Cowl IV_a; diffuser total-pressure recovery, 0.651; catpured-mass-flow ratio, 0.91.

(b) Cowl IV_b; diffuser total-pressure recovery, 0.571; captured-mass-flow ratio, 0.91.

Figure 24. - Schlieren photographs of isentropic inlets with no internal contraction at supercritical flow conditions. Spike IV_a; spike-tip position, 24.91°; free-stream Mach number, [illegible]; Reynolds number, 0.45×10^6.

NACA-Langley - 3-26-54 - 325